ELIMÄKI locus is required for vertical proprioceptive response in birch trees

Juan Alonso-Serra[1,2†], Xueping Shi[3*], Alexis Peaucelle[4,5*], Pasi Rastas[2*], Matthieu Bourdon[4*], Juha Immanen[1,2,6], Junko Takahashi[7], Hanna Koivula[8], Gugan Eswaran[1,2], Sampo Muranen[1,2], Hanna Help[9], Olli-Pekka Smolander[2,10], Chang Su[1,2], Omid Safronov[1,2], Lorenz Gerber[7,11], Jarkko Salojärvi[1,12], Risto Hagqvist[6], Ari Pekka Mähonen[1,2], Ykä Helariutta[1,2,4††] and Kaisa Nieminen[6†].

Affiliations:

[1] Organismal and Evolutionary Biology Research Program, Faculty of Biological and Environmental Sciences, Viikki Plant Science Centre, University of Helsinki, Helsinki, 00014, Finland.
[2] Institute of Biotechnology, HiLIFE, University of Helsinki, Helsinki, 00014, Finland
[3] Key Laboratory of Horticultural Plant Biology of Ministry of Education, College of Horticulture and Forestry Sciences, Huazhong Agricultural University, Wuhan, 430070, China.
[4] Sainsbury Laboratory, University of Cambridge, Cambridge, CB2 1LR, United Kingdom.
[5] Institut Jean-Pierre Bourgin, INRA, AgroParisTech, CNRS, Université Paris-Saclay, 78000, Versailles, France.
[6] Production systems, Natural Resources Institute Finland (Luke), 00790, Helsinki, Finland.
[7] Umeå Plant Science Center, Department of Forest Genetics and Plant Physiology, Swedish University of Agricultural Sciences, Umeå, 901 83, Sweden.
[8] Department of Food and Nutrition, Faculty of Agriculture and Forestry, University of Helsinki, Helsinki, 00014, Finland.
[9] Department of Physics, Division of Materials Sciences, X-ray Laboratory, University of Helsinki, Helsinki, 00014, Finland.
[10] Department of Chemistry and Biotechnology, School of Science, Tallinn University of Technology, Tallinn, Estonia.
[11] Genome Institute of Singapore, 138672 Singapore.
[12] Singapore Centre for Environmental Life Sciences Engineering, Nanyang Technological University, 63755, Singapore.

***** These authors contributed equally
† Corresponding authors
††Lead contact

Correspondence: Juan Alonso-Serra: juan.alonsoserra@helsinki.fi, Ykä Helariutta yrjo.helariutta@slcu.cam.ac.uk and Kaisa Nieminen: kaisa.p.nieminen@luke.fi.

Summary

Tree architecture has evolved to support a top-heavy above-ground biomass, but this integral feature poses a weight-induced challenge to trunk stability. Maintaining an upright stem is expected to require vertical proprioception through feedback between sensing stem weight and responding with radial growth. Despite its apparent importance, the principle by which plant stems respond to vertical loading forces remains largely unknown. Here, by manipulating the stem weight of downy birch (*Betula pubescens*) trees, we show that cambial development is modulated systemically along the stem. We carried out a genetic study on the underlying regulation by combining an accelerated birch flowering program with a recessive mutation at the *ELIMÄKI* locus (*EKI*), which causes a mechanically defective response to weight stimulus resulting in stem collapse after just three months. We observed delayed wood morphogenesis in *eki* compared with WT, along with a more mechanically elastic cambial zone and radial compression of xylem cell size, indicating that rapid tissue differentiation is critical for cambial growth under mechanical stress. Furthermore, the touch-induced mechanosensory pathway was transcriptionally misregulated in *eki*, indicating that the *ELIMÄKI* locus is required to integrate the weight-growth feedback regulation. By studying this birch mutant, we were able to dissect vertical proprioception from the gravitropic response associated with reaction wood formation. Taken together, our study provides evidence for both local and systemic responses to mechanical stimuli during secondary plant development.

Key words: trees, mechanosensing, proprioception, radial growth, forward genetics, wood formation, *Betula*.

Introduction

Trees are recognizable by their great, but not unlimited, height and diameter. Two meristems control the final stem dimensions: the radial growth derives from activity of the vascular cambium, while the apical growth of stem depends on the shoot apical meristem (SAM). The stem size is further increased by the internode elongation and the intrusive growth of cambium derived cells [1, 2]. Thus, the development of large-scale organs constitutes an inherent mechanical challenge to the meristematic tissues they originate from.

The activity of the plant apical meristems is known to be controlled by intrinsic mechanical forces: deformation, the stretching and/or compression of plant tissues, has a direct impact on organ morphogenesis[3–5]. Similarly, mechanical signals appear to impact radial growth: a decrease in pressure on the tree stem cambium inhibits vascular tissue production, whereas an increase in pressure promotes cambial activity and xylem differentiation[6, 7]. During secondary growth, cambium-derived tissues of a tree stem additionally experience maturation stress, a combination of

lateral compression by the restricting outer tissues and expanding inner ones [8]. The highest mechanical stress is experienced at the base, which holds the complete loading of the aerial plant body weight. Thus, the maintenance of cell wall integrity during wood morphogenesis is intrinsically important for the mechanical support of the stem[1, 9].

Since the weight of above-ground biomass correlates positively with stem diameter[10], the existence of a vertical proprioception, a mechanism that would sense and balance radial growth systemically with the weight increase of an upright tree, has been hypothesized [11]. In this circuit, allometry, the allocation of biomass along the stem, would be systemically affected by mechanical stress of the stem's own weight. Two main theories have been formulated about the mechanisms controlling the allometric growth of an upright tree stem. The growth-hydraulic theory states that the scaling between height and diameter derives from hydraulic constraints; there is a limit to how much water can be transported by a certain stem diameter[12]. The mechanical theory states that the taller a stem gets compared to its basal width, the greater the risk of weight- or wind-induced buckling, thereby providing an evolutionary selective pressure to avoid mechanical damage[13]. In the nature, external stimuli, such as wind or touch, can also trigger a developmental response called thigmomorphogenesis, often manifested by restricted apical growth and increased secondary growth of the shoot[14, 15]. In a gravitropic response to a disturbance of stem curvature or posture the altered orientation triggers locally corrective reaction wood formation[16, 17]. Together these internal and external forces affect the final shape and dimensions of developing organs.

Given that the increase of stem weight is a common element to all scenarios, we here first studied whether changes in vertical loading can serve as a mechanical cue to control secondary growth in trees. Then, by implementing a fast forward genetics approach in birch, we identified within four years a single recessive locus (*EKI*) required for radial growth response to weight. Finally, we showed that the timely acquisition of xylem biomechanical stiffness is critical for coping with lateral and vertical mechanical stress during vertical proprioception.

Results

Vertical loading stimulus systemically modulates radial growth in a tree stem

To gain experimental insight into the impact of weight-derived vertical forces on secondary growth, we studied the effect of weight modifications on stem allometry by adding or relieving 75% of the predicted weight in the upper half of a WT birch stem. Four treatments were implemented: a supported control stem with no added weight (C1); weight added to a supported stem (C2); weight added to a semi-supported stem capable of limited lateral movement (C3); and a stem pulled up from the top (C4) (Figure 1A and B). The stem response to each treatment was followed for three weeks by measuring the diameter of the four downmost internodes at the stem base (D1-D4),

together with internodes at the 50% (D5), 62.5% (D6), and 75% (D7) of stem height (Fig. S1). The radial growth rates are given as percentage increments relative to the diameter of each internode at the beginning of the experiment (T1) (Figure 1, S1 and Data S1A).

The three weight manipulations (C2, C3 and C4) affected stem allometry by making the relative radial growth rate significantly higher at the upmost measured internode D7 compared to the downmost D1, producing a top-to-bottom gradient of decreasing growth rates (Figure 1E and Data S1B). By comparing the combined radial growth rate in the upper internodes (D5-D7) between treatments, calculated by pooling together the growth rate of each internode during the whole experiment (between timepoints T1-T4), a significant difference was observed for semi-supported stems (C3) compared to supported control (C1) (Data S1B). At the stem base (D1-D4), the radial growth rate was significantly increased in semi-supported (C3) compared to supported stems (C2) (Figure 1C and E). None of the mechanical treatments induced tension wood development, indicating that the observed radial growth responses to stem loading occurred through the adjustment of normal wood formation. The apical growth rate was enhanced by all treatments; the strongest significant effect was seen by pulling (C4) (Figure 1D). However, no differences were detected between weight-treated supported (C2) and semi-supported (C3) trees, indicating that their apical and radial growth responses were uncoupled. Moreover, the increase in the internode number was similar in all treatments (Figure S1D), indicating that while some of the treatments promoted internode elongation, they did not induce new organ production at the SAM, further supporting their differential effects on apical and radial growth.

The adjustment of radial growth in response to the sensing of a mechanical stress, caused by an alteration in stem weight, conforms to the principle of the proprioception feedback loop[18]. Since the radial growth rate was increased more in the semi-supported than in the supported trees, our results indicate that lateral movement serves as a mechanical cue to transmit the vertical loading stimulus into a radial growth response at the stem base, likely by enhancing the mechanical deformation of basal stem tissues. Since in our experimental setup trees were always standing upright and subjected to only vertical forces from the weight manipulations, we define this mechanism as vertical proprioception.

Fast-forward genetics with birch identifies a single *ELIMÄKI* locus linked to stem mechanics

To study the developmental relevance of the observed proprioceptive response, we investigated a loss-of-function *Betula pubescens* mutant phenotype, "*Elimäki Original*" (*EO*) (Figure 2A). The original, ca. 70-year old mutant tree has a short and bushy phenotype with many broken branches; stems of clonal mutant seedlings provide insufficient support and collapse after only three months of growth (Figure S1F). In *Betula* species, specific greenhouse conditions can accelerate flowering

to under one year[19], enabling us to generate a segregating mapping population to study the mutant. Seeds from wind-pollinated, out-crossed flowers (F_1) produced WT-like, upright-standing trees (Figure 2A), whereas self-pollinated EO progeny trees (S_1) collapsed (Figure S1G). By crossing an F_1 individual with EO, we generated a backcross population (BC_1) of 60 trees. The number of upright standing (WT) vs. suddenly (approximately 60 Days After Potting [DAP]) collapsing *elimäki* (*eki*) phenotypes fit a 1:1 segregation ratio (Video S1, Figure 2A and Data S2), revealing that *eki* segregates as a recessive monogenic locus. Ploidy estimates using flow cytometry, together with a previous genome analysis[20] confirmed that EO belongs to a tetraploid *B. pubescens* (4n=56) species (Figure S2). To identify a genetic association, the genomes of BC_1 trees and their parents were individually sequenced and mapped to the available *B. pendula* genome[20] . A linkage map with about 2.5 million simplex (AAAB x AAAA) markers and 56 linkage groups (likely 4n=56) was constructed (Figure S2N). QTL mapping identified the *ELIMÄKI* locus (*EKI*) at the end of chromosome 11 in the BC_1 population and to a specific linkage group in the EO parent (Figure 2B and C). The identified mapping window contains 324 annotated genes in the *B. pendula* genome (Data S2C).

The *ELIMÄKI* locus is required for the proper radial growth responses during vertical proprioception

Time-scale profiling of radial growth along the stem revealed that the basal diameter of an *eki* tree was smaller than in WT at the final time-point before collapse (Figure 3A, B and S3). *eki* trees appeared unable to adjust their radial growth rate in response to their increasing size. We therefore tested whether radial growth was compromised in *eki* in a weight-dependent manner. In contrast to the WT control treatment (C1), where the diameter increase along the stem was stable, preserving allometric growth, the profile in *eki* was more variable (Figure 1E). The variation was calculated as coefficient of variation (CV), based on the relative growth rates of each measured internode (D1-D7) along the stem. While adding weight promoted radial growth in the upper internodes of *eki*, this was not was not case at the base of semi-supported stems (C3) (Figure 1C-E, Figure S1, Data S1A and B), indicating that the basal tissues of *eki* plants were less responsive towards weight stimulus. By relieving some of the weight stress via pulling (C4), we were able to reduce the variations in the radial growth rate between the internodes in *eki* stems compared to supported control (C1), indicating that the deviation from normal allometric growth in C1 was partly weight-based (Data S1B). No tension wood was observed in *eki* stems before their collapse (Figure S4). Following it, *eki* main stems and side branches produced tension wood and grew upwards in a gravitropic manner, only to collapse again after reaching a critical size (Figure S3D and E). The trees eventually developed a bushy phenotype resembling the original EO tree. The observation of a fully functional gravitropic response in *eki* trees confirms the distinction between intrinsic vertical proprioception response involving normal wood formation and a gravitropic response to tilting. Taken together, the weight-

induced radial growth response at the base of WT (Fig 1E, C3 vs. C2), and the lack of such response in *eki*, indicate that a growth adjustment for changes in the above-ground weight is important for the maintenance of vertical stem posture in trees and that the *EKI* locus is required for this response.

Lateral compression of wood morphogenesis increases along the tree size

To understand the cellular basis of the impaired proprioceptive response in *eki*, we studied the morphogenesis of woody tissues in progressive developmental stages along the stem. In line with the smaller diameter of the oldest internodes at the base (60 DAP), *eki* tissues had fewer xylem cells than WT, and the cross-sectional area of individual xylem fibers was smaller (Figure 3E and F). Given the large reduction in diameter (2.22±0.47 mm) and the relatively small decrease in cell number (15±4 cells ~ 242±64μm, Data S1C), the smaller diameter at the base of *eki* stems was likely due to defective xylem cell expansion rather than the decreased cell number. Analysis of xylem morphology additionally revealed concentric sectors of smaller cells at the base of *eki* stems (Figure 4). However, at middle heights in the stem this defect was partial and the cross-sections showed compression only close to the cambium, indicating that cell size compressed progressively along the stem axis from internodes at middle height to the older ones at the base. Unexpectedly, in contrast with the basal phenotype, the younger and higher internodes below the apex of 60 DAP *eki* trees had more xylem development than WT (Figure S3G). Even one-month old *eki* trees (30 DAP) with ca. 15 cm. long main stem (Figure S1A) showed an increased number of xylem cells in upper internodes, and the size of an individual fiber cell was larger than in WT (Figure 3C, D and S3F). Combined, these results suggest that the phenotypes associated with vascular compression developed as trees grew in size. Thus, the *EKI* locus appears to have context dependent effects on wood development: it restricts xylem cell proliferation and expansion in young internodes but promotes them in the older ones. Consistent with this, during wood morphogenesis in *eki* we observed stronger and more widespread symptoms of maturation stress than are normally seen at the base of an upright standing tree, where the vertical mechanical stress is at its highest.

***ELIMÄKI* locus is required for mechanical stiffening of the wood-forming zone**

Since the local mechanics of weight-derived forces on radial growth are poorly known, we produced the first tissue-specific elastic modulus map across the wood-forming zone by performing atomic force microscopy (AFM) indentations (Figure 4E). In WT trees, differentiating xylem and phloem tissues rapidly acquired a high Young's modulus, thereby becoming stiffer than the mechanically soft cambium. In *eki*, the area of softer tissues was wider and reached further into developing xylem and phloem tissues, becoming unevenly stiffer only later in the xylem. Accordingly, *eki* internodes were weaker than WT in the bending test, independent of stem diameter (Figure 4F and G). Together, these results show that the wood-forming zone was mechanically softer in *eki* and that

local defects in a mechanically-stressed cambial environment can have large consequences for the postural control of a tree stem.

Correct timing of xylem differentiation is critical for radial growth under mechanical stress

To connect the measured elasticity with secondary cell wall development, we studied both cell wall composition and deposition across the wood-forming zone. We performed high-throughput cell wall profiling of wood and bark from both young and mature internodes to quantify cellulose, hemicelluloses and lignin. We identified only subtle and non-specific alterations between *eki* and WT in the content of guaiacyl lignin, syringyl lignin, xylose, non-cellulosic glucose, arabinose and mannose and no difference in total cellulose (Figure S5).

Next, we investigated potential differences in the progress of cell wall development during wood morphogenesis. Cellulose deposition and lignification in differentiating xylem tissues were delayed in *eki* compared with WT (Figure 5 A, B, and C). We therefore investigated the localization of pectin, which is a major component of undifferentiated or developing xylem and phloem tissues[1] (Figure 5D, E, F and S6). We observed a pectin gradient across the cambial zone in WT, extending from the conductive phloem into the developing xylem. This gradient was notably wider in *eki*, reaching further from the outer phloem parenchyma cells deeper into the maturing xylem tissue. These analyses indicate that secondary cell wall deposition was delayed in *eki*, since differentiating tissues retained primary cell wall characteristics longer. Such a pattern is consistent with the mechanical softness of *eki* tissues. Moreover, the delayed differentiation of vascular tissues was becoming more pronounced towards the stem base (Figure S6), coinciding with the maturation stress phenotype of concentric sectors of small cells. Since we observed only subtle differences in our bulk xylem cell wall composition analysis, our results indicate that a highly accurate spatio-temporal deposition of secondary cell walls is critical for wood morphogenesis under vertical mechanical stress.

***ELIMÄKI* locus is transcriptionally associated with touch-induced mechanosensing pathways.**

In order to identify the transcriptomic differences between WT and *eki* trees, we compared differentially expressed genes (DEGs) at two upper stem positions, internode 2 (IN2), which is morphologically similar in both genotypes, and IN5, where enhanced xylem differentiation is evident in *eki* (Figure 6 and S4). To address tissue specificity, the lower internode was dissected into bark and xylem samples. In all samples, DEGs were significantly enriched for the GO terms “mitochondrial stress“, “component of mitochondrial membrane”, “respiratory burst” and “jasmonic acid biosynthesis”; xylem samples were also enriched in “plant-type cell wall” (Figure 6 and Data S3). A similar molecular profile has recently been associated with the mechanosensory touch-response in *Arabidopsis*[21–23], and orthologues of 12.3% of the 1107 *Arabidopsis* touch-affected genes[22] were differentially expressed between *eki* and WT (Figure 6E), including touch-inducible genes

(*WRKY15*, *WRKY40* and *OM66*), mitochondrial stress markers (*AOX1a*), and genes required for touch-induced developmental responses (*AOX*[21] and *VIP3*[24]). This molecular signature highlights how central mechanosensory pathways are transcriptionally affected in *eki* trees. Even though some of the touch-responsive genes were in the mapping window (Data S2C), our results indicate that the *EKI* locus controls the expression of touch-responsive genes *in trans,* thus modulating globally a central mechanosensing pathway.

Discussion

In contrast to the previous studies describing the developmental responses triggered by external forces, such as wind, touch or tilting, our aim here was to explore the proprioceptive response to the vertical stress produced by the weight of an upright stem. We observed that an increased weight stimulated cambial activity at the base of semi-supported WT trees, whereas such a response was absent in *eki*, a birch mutant unable to maintain an upright stem posture. Interestingly, without added weight *eki* trees had more cambial activity than WT in the upper stem, and less cambial activity at the base. This observation indicates that correct allometric growth is retained in WT trees through the *ELIMÄKI* locus. Our interpretation is that, regarding the stem position, the proprioceptive signal affects cambial activity in a context dependent manner: it promotes radial growth at the base for a weight increase while it controls the allometry of radial growth along the stem.

The integrated phenotype characterization of *eki* trees indicated that initial differentiation steps during radial growth such as secondary cell wall deposition were compromised, making these tissues mechanically softer. While the *in situ* cell wall analyses revealed a delay in xylem differentiation, the bulk cell wall profiling revealed only subtle differences. This difference may be attributed underrepresentation of affected tissues in our samples, while it also highlights that final cell wall composition was only slightly affected in *eki*. Moreover, these cell wall defects seemingly impacted on the mechanical characteristics of woody tissues. Defective cell walls could explain the compression and number reduction of xylem cells at the base of *eki*, given that these tissues support the complete aerial stem weight. Since the incapacity to respond to added weight at the base of *eki* stem may be linked to the delayed secondary cell wall formation, further studies are required to dissect the contribution of cell wall development to the impaired proprioceptive response. However, we observed that the *eki* trees have a normal reaction wood response, suggesting the *ELIMÄKI* locus is mainly required for responses in vertically standing trees. Consequently, we find that the *eki* mutation is informative for the proprioceptive response in these various contexts.

Altogether, our results highlight a regulatory circuit by which weight in tree trunks mechanically stimulates cambial growth. The *ELIMÄKI* locus participates in this circuit, as shown by its

requirement at various levels, from weight-induced growth response to the proper control of gene expression related to touch-induced mechanosensing. The circuit facilitates the local acquisition of the biomechanical characteristics of xylem in the correct spatio-temporal manner, which systemically leads to a correct vertical proprioception response. It remains to be studied how weight- and development-derived forces are sensed and transduced into radial growth, but our results indicate a critical role for a degree of lateral stem movement. Similarly, it remains to be studied in the future whether the *ELIMÄKI* locus contributes directly to the sensing of the proprioceptive signal or it is only part of its response. Taken together, our results provide a mechanism through which the critical height-diameter ratio implied by the mechanical theory of tree evolution can be achieved. Finally, it is worth highlighting that to characterize and map the *ELIMÄKI* locus, we produced a backcrossed segregating population starting from a naturally occurring mutant within four years, thus introducing *Betula* as a model for forward genetic tree studies.

Acknowledgements:

The authors are grateful for the excellent technical assistance of Katja Kainulainen, Wouter Beijk, Rebecca Kramps and the Biopolymer Analytical Platform (BAP) at Umeå Plant Science Centre. We thank Sedeer el-Showk for proof-reading the text. This study was supported by the Academy of Finland Finnish Centre of Excellence in Molecular Biology of Primary Producers (CoE 2014-2019) project (271832) and the project (286404), the Gatsby Foundation (GAT3395/PR3), the University of Helsinki (799992091), and the European Research Council Advanced Investigator Grant SYMDEV (323052).

Authors Contribution:

Y.H, K.N and J.A.S, designed the research; J.A.S, X.S, A.P, P.R, M.B, J.I, J.T, H.K, G.E, S.M, H.H-R-R, O-P.S, C.S, R.H, A.P.M and K.N performed the research; J.A.S, X.S, A.P, P.R, M.B, J.I, J.T, H.K, G.E, O-P.S, L.G, O.S, J.S and K.N analyzed the data; and J.A.S ,Y.H and K.N wrote the paper.

Declaration of interests

The authors declare no competing interest

Main Figure Legends

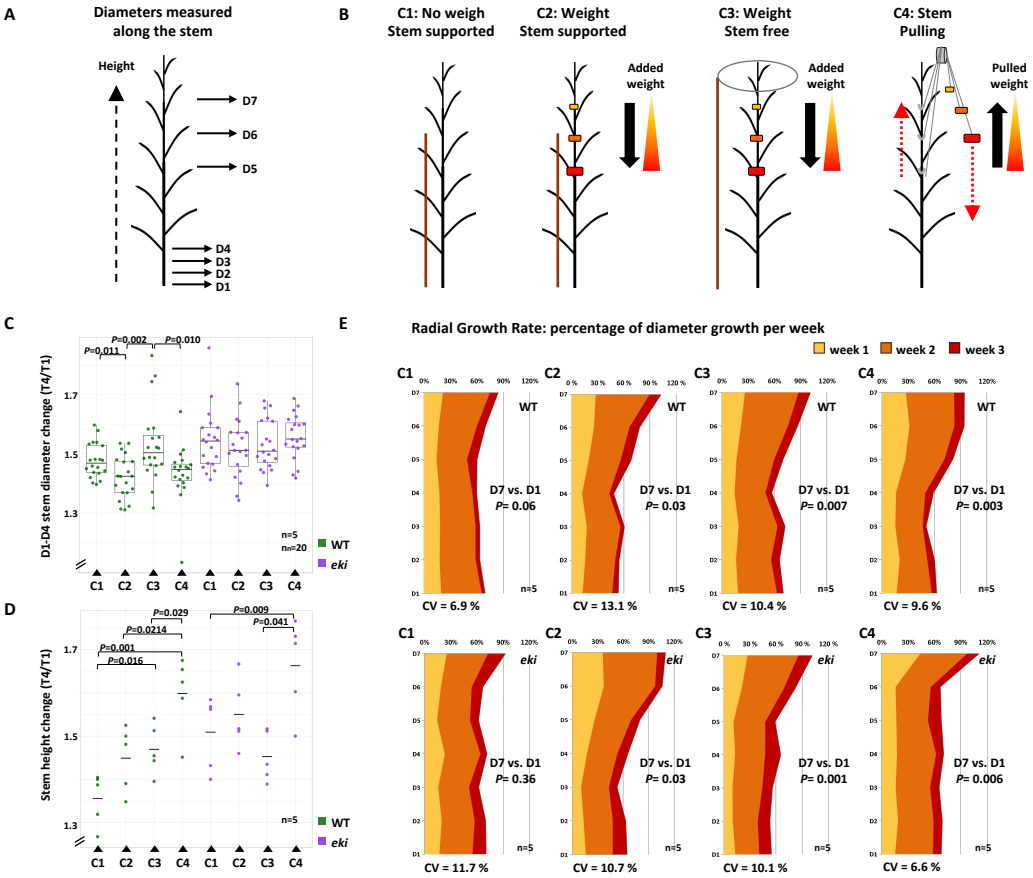

Figure 1. Stem weight manipulations affect the rate of radial growth. A) Diagram showing the measured stem positions: D1-D4, diameters of four downmost internodes at the stem base. D5, D6 and D7, diameters at the positions of 50%, 62.5% and 75%, respectively, of stem height. **B)** Experimental setup for vertical mechanical manipulations of stem weight: Condition 1 (no weight treatment on supported stems), Condition 2 (weight added to supported stems), Condition 3 (weight added to semi-free stems), Condition 4 (stems pulled up from the top). Black arrows indicate the direction of mechanical stimuli and red arrows indicate the pulling direction. Diameters were recorded at 4 timepoints (T1-T4) and, to imitate the natural loading distribution, the weight was applied through a gradient **C)** Stem diameter ratio equivalent to percentual growth rates (1.5 = 50%) between the final and initial time-points (T4/T1) combining the downmost 4 internodes from the base (D1-D4), n=biological replicates, n_n=samples. **D)** Stem height ratios equivalent to percentual growth rates (1.5 = 50%) in T4/T1 from the same trees shown in C. In all boxplots, the box indicates the interquartile range (IQR), the whiskers show the range of values within 1.5*IQR, and a horizontal line indicates the median. Statistically significant differences between WT and *eki* ($p \leq 0.05$) were determined by a two-tailed Student's t-test and are indicated in the plots. **E)** Radial growth rates showing the percentage of diameter growth per week (relative to the initial diameter, T1) at each vertical stem position. The plots correspond to the conditions illustrated above in WT and *eki* and represent averages. Coefficient of variation (CV) was calculated using the total growth percentage (at T4) of all internodes and replicates (Data S1). Each experimental setup consisted of 5 trees per treatment (See Data S1).

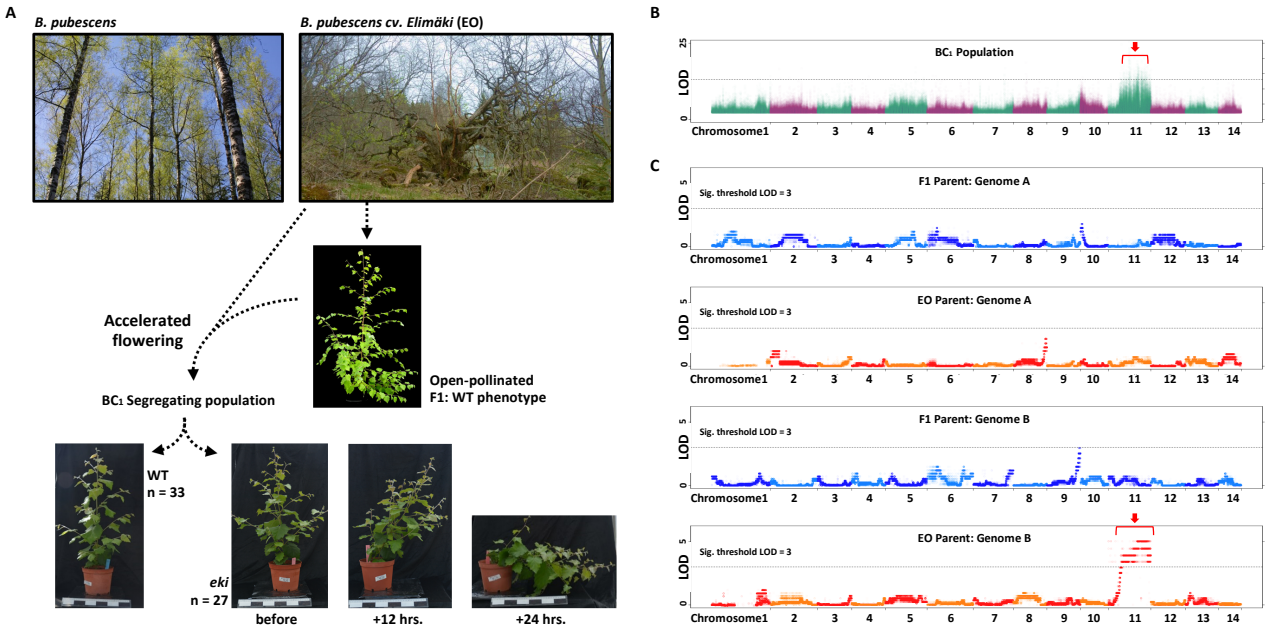

Figure 2: A stem mechanics mutant identified by forward genetics in birch. A) Downy birch (*B. pubescens*) typically grows as a single straight-stem tree, whereas the naturally occurring mutant *B. pubescens cv. Elimäki (EO)* has distinctive stem architecture with multiple irregular branches. Open-pollinated F1 individuals had the WT phenotype. A 2-year old F1 was induced to flower and backcrossed with EO to produce 60 BC_1 trees with a 1:1 segregation for the WT vs. collapsing phenotype. The *eki* trees have normal vertical growth for three months until they start to tilt and collapse in less than 24 hrs. (see Video S1, Figure S1 and S3) **B)** A Manhattan plot showing the association of polymorphic markers with the *ELIMÄKI* locus in chromosome 11 using the *B. pendula* genome as a reference. Markers from WT and *eki* individuals in the BC_1 population were separately pooled. The candidate mapping window is indicated by a red arrow. **C)** A Manhattan plot showing the association of polymorphic markers with the parents F1 (WT phenotype) and EO (*eki* phenotype). The tetraploid genome was separated into Genome A and Genome B (see also Figure S2). The horizontal dotted line indicates the significance cutoff for the identified associations. The *Betula pubescens* picture was provided by Erkki Oksanen (Luke-Finland).

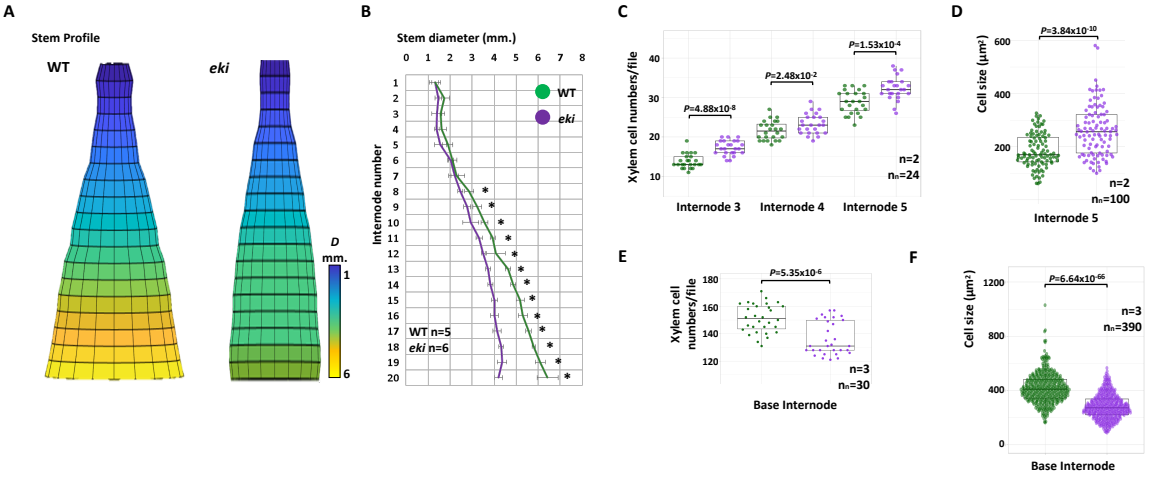

Figure 3. Cell size variations in *eki* are dependent on the stage of stem development. A) The allometry of radial growth reconstructed from the diameters shown in **B**, with each horizontal line corresponding to one internode (error bars = SD). The profiles highlight the decreased thickening slope in *eki* trees (see also Figure S1, S3 and S4). **C)** Xylem cell numbers per individual xylem cell file in young internodes (30 DAP). **D)** Cell size of xylem fibers in young internode 5 (30 DAP): The

box plot illustrates the overall larger size in *eki* compared to WT. **E)** Xylem cell numbers per individual xylem cell file in the older internode at the base (60 DAP) **F)** Cell size of xylem fibers at the older stem base (60 DAP): The box plot illustrates the overall smaller size in *eki* compared to WT. In all boxplots, the box indicates the IQR, the whiskers show the range of values within 1.5*IQR, and a horizontal line indicates the median. Statistically significant differences between WT and *eki* ($p \leq 0.05$) were determined by a two-tailed Student's t-test and are indicated in the plots or marked with asterisks. n=biological replicates, n_n=samples. (See Data S1)

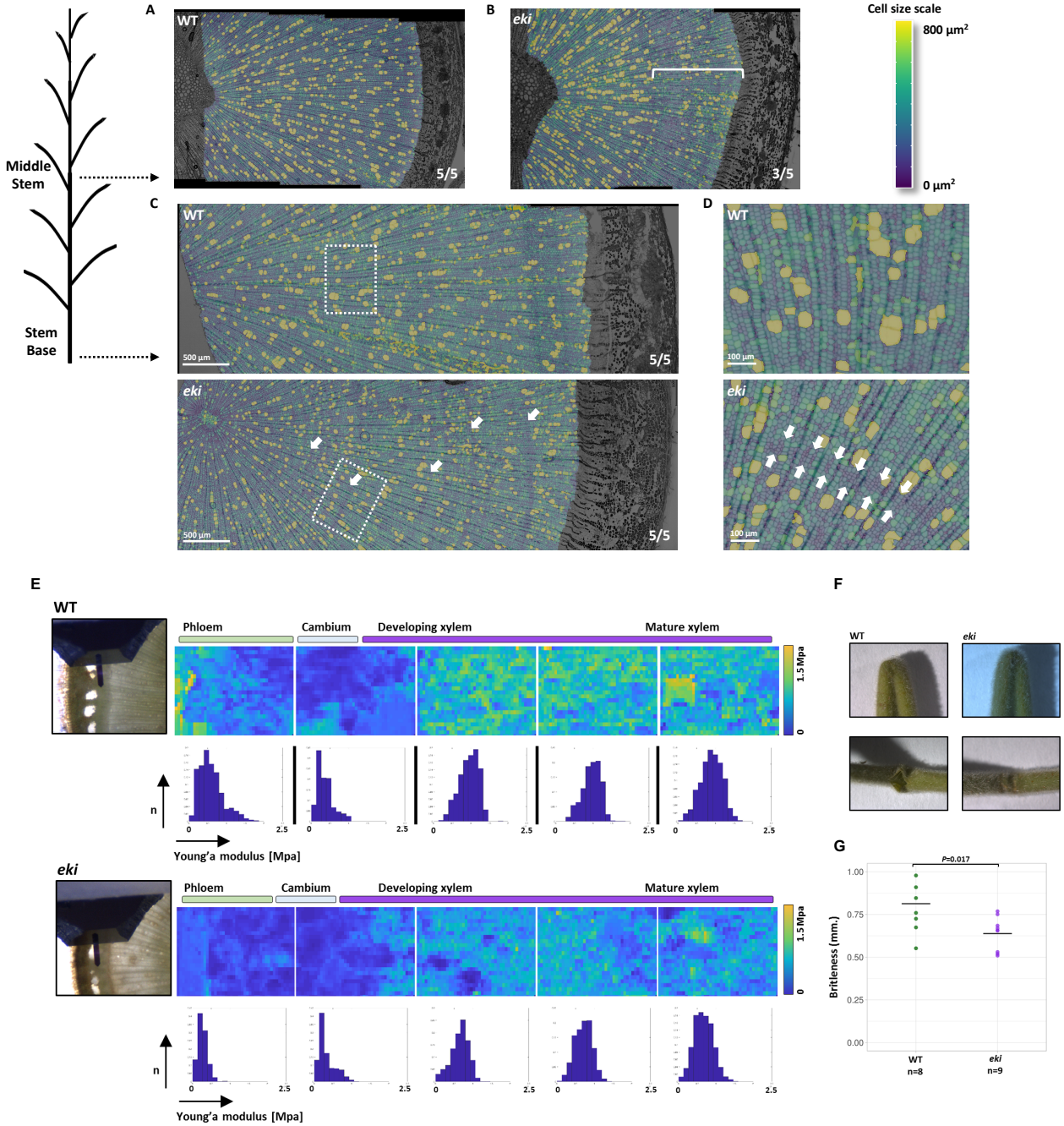

Figure 4. The compression of xylem fibers in *eki* coincides with a lower tissue elastic modulus of differentiating woody tissues.

A-D) Anatomical images were segmented with LithoGraphX and overlaid with heatmaps corresponding to cell size (μm^2). The schematic indicates the analyzed stem positions. Stem cross-sections were taken at middle height **(A-B)** and at the base **(C)**. **D)** Magnified image from the white

boxes in C. White bracket marks a sector of compressed cells at middle height and white arrows indicate concentric rings of small cells at the base. Occurrence frequency of the shown pattern is indicated. **E)** Tissue-specific mechanical properties determined by AFM measurements of Young's modulus across the cambial zone, from phloem to mature xylem tissues in WT (top) and *eki* (bottom). Fresh middle-height cross-sections were used. A stereoscope image was acquired before each AFM run to localize the tissues (image shown corresponds to the first map). Heatmaps are representative of 13 WT and 14 *eki* stem cross-sections analyzed by two independent measurements. The color scale goes from 0 to 1.5 MPa. Histograms in the lower panels illustrate the distribution of Young's modulus values for each map. **F)** The outcome of manual bending of stem internodes of similar diameter (⌀2.8mm ± 0.27): when fresh stems were manually bent, the bark of WT internodes broke, whereas the *eki* did not break and appeared to be more flexible. **G)** Brittleness test: In order to assess the lateral tensile strength of internodes, we dehydrated stem sections and performed a three-point bending test. The *eki* internodes were significantly more brittle than WT. Samples had similar diameter and brittleness values were diameter normalized in three biological replicates. Data is shown in a dot plot with the horizontal line indicating the mean. Result of a two-tailed Student's t-test is indicated.

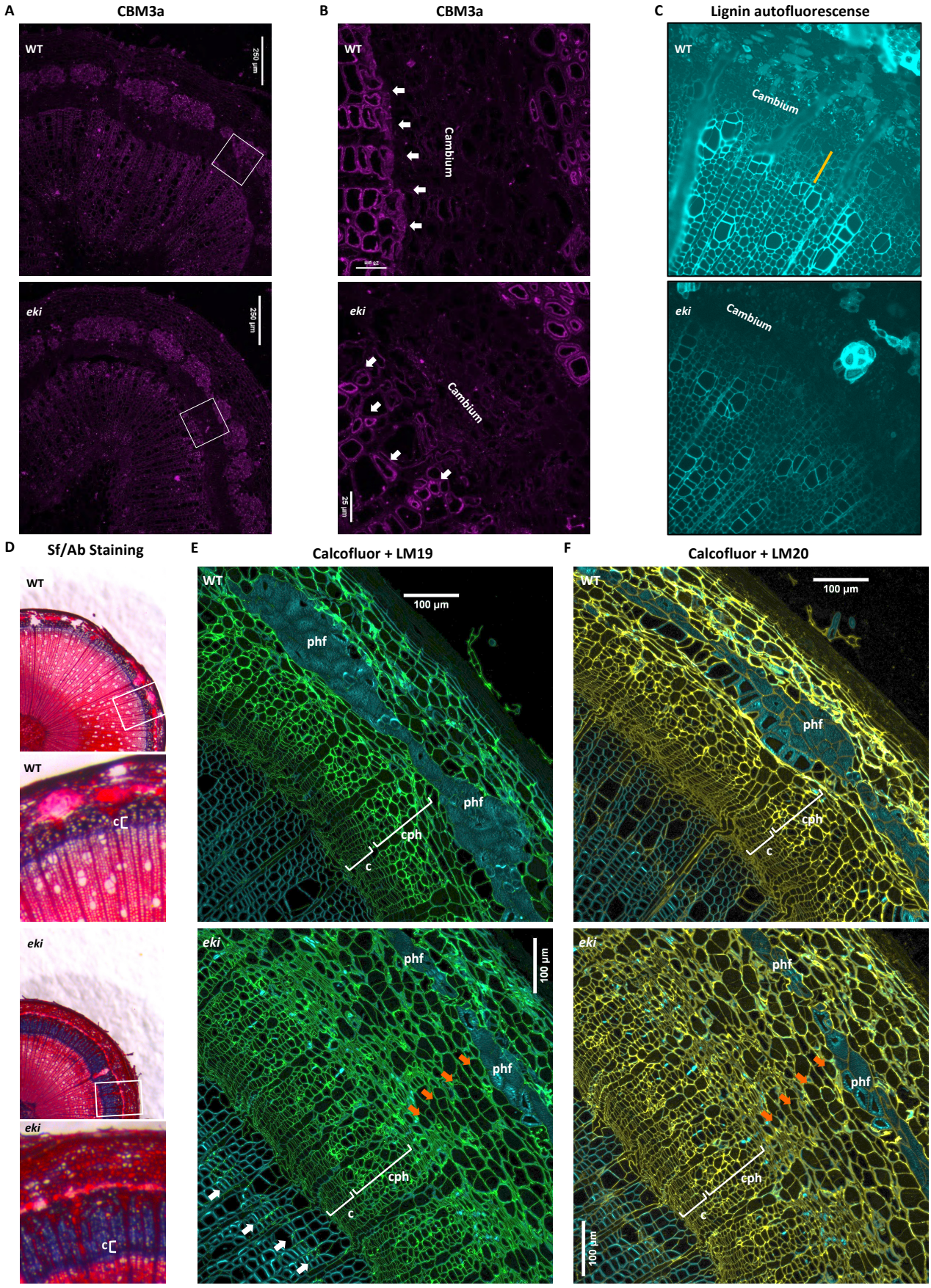

Figure 5. Xylem differentiation is delayed in *eki*.

A) Immunolocalization of crystalline cellulose by CBM3a in stem cross-sections. **B)** Magnification from white boxes shown in A. White arrows indicate the first developing xylem cells. **C)** Visualization of lignin by UV autofluorescence. The orange line indicates the narrow sector of non-lignified developing xylem fibers in WT; the initiation of lignification is delayed in *eki*. **D)** Cryosections from the stem base stained with alcian blue dye for acidic and pectin-like polysaccharides and safranin for lignified cell walls. WT cross-sections had only a narrow alcian blue stained sector within the cambium zone, whereas a broader area, expanding from phloem to the developing xylem, was seen in *eki*. Lower panels are magnifications from the white boxes shown above. **E-F)** Immunolocalization of homogalacturonan by LM19 (E) and LM19 (F) at the stem base. Image colors correspond to calcofluor white counterstaining (cyan), LM 19 (green) and LM20 (yellow). Conductive phloem (cph). Phloem fibers (phf). White and orange arrows indicate the extended LM19 and LM20 labeling in xylem and phloem of *eki* trees (see also Figure S5 and S6).

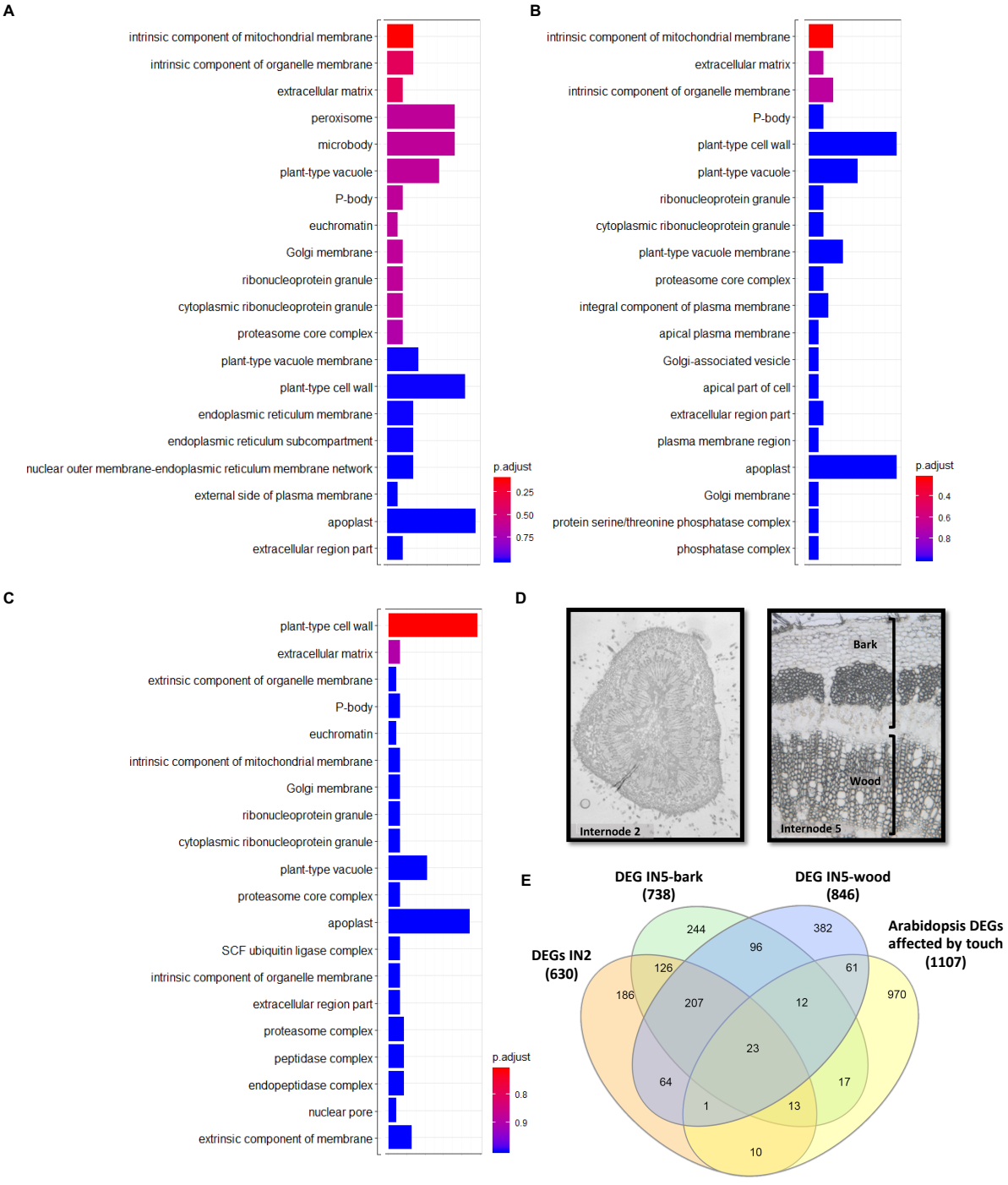

Figure 6: The touch-induced mechanosensing pathway is transcriptionally misregulated in *eki*. A-C) GO categories associated with cellular components in **A)** internode 2, **B)** IN5-bark and **C)** IN5-wood. **D)** Microscope images representative of the analyzed tissues. **E)** A Venn diagram of *Arabidopsis* orthologues of birch DEGs in IN2, IN5-bark and IN5-wood compared to the list of touch-induced genes in *Arabidopsis*[22]. The overlapping DEGs include key touch-induced genes, mitochondrial stress markers and genes required for the *Arabidopsis* thigmomorphogenesis response. (See Data S3).

STAR Methods

LEAD CONTACT AND MATERIALS AVAILABILITY

Further information and requests for resources should be directed to and will be fulfilled by the Lead Contact: Ykä Helariutta (yrjo.helariutta@slcu.cam.ac.uk). This study did not generate unique reagents

EXPERIMENTAL MODEL AND SUBJECT DETAILS

The cultivar *Betula pubescens cv. Elimäki* (EO) is located in: 60° 45' 4.4892"N, 26° 29' 21.282"E and was identified by Natural Resources Institute Finland (Luke ID: E11431). Individuals 14-038-01 (*eki*), 14-038-22 (*eki*), 14-038-58 (WT) and 14-038-17 (WT) were established *in vitro* and clonally propagated as previously described[25] and grown under normal greenhouse conditions (22-25 °C,18 hrs light) with automatic watering. Unless otherwise indicated in the figure legends, the analysis of trees was performed in 3-month-old trees or before the collapse of mutant individuals.

METHODS DETAILS

Induced early flowering and crossings:

The natural flowering period for birch in southern Finland is spring (April to May), when trees break dormancy. In the first year (2011) the identified cultivar *Betula pubescens cv. Elimäki* (EO) was selfed by performing controlled crossings to produce S1 trees. Briefly, branches with dormant male flowers were bagged with pollination bags (model: 2D-1-1W, from PBS International, UK) during March 2011. Within the following weeks the male flowers burst and the female flowers emerged inside the closed bags, evenutally producing S1 seeds. F1 trees were obtained by collecting wind-pollinated seeds from EO (July-August 2012). All seeds were allowed to ripen on the tree, air dried for 5 days and stored in a -5 °C freezer for at least one month. In March 2012, seeds were planted and trees were grown under normal greenhouse conditions (18 hrs DL), then put into dormancy (October 2012) by allowing greenhouse rooms to acclimate to outdoor conditions. In total, 21/21 F1 trees had the WT phenotype, and 15/15 S1 trees had the mutant phenotype. Flowering of F1 trees was induced using a previously published protocol[19] in February 2013 when there was no registered ambient

pollen. Briefly, dormant trees were placed in a room with long-day light conditions, constant 25°C and CO_2 gas was released until the concentration reached 1200-2000 ppm. Flowering was successfully induced (2013), but these seeds didn't germinate. The following year, F1 flowering was successfully induced again (February 2014), producing viable seeds. After visible female flowers emerged, branches were bagged and pollinated by injecting EO pollen. Seeds were allowed to ripen on the branch, air dried and stored in a -5 °C freezer for at least one month. The BC_1 population was then grown from seeds in February 2015. The BC_1 population consisted of 60 trees, of which 33 had a WT phenotype and 27 an *eki* phenotype (Data S2).

Vertical mechanical manipulations:

The vertical mechanical manipulations consisted of 4 different experimental setups. Weight treatments were performed by manipulating the equivalent of 75% of the weight in the upper half of the stems. This weight was estimated by cutting stem sections from 3 WT and 3 *eki* trees and measuring their weight, then using this information to calculate the respective 75% weight of WT or *eki*.

Weight was applied using handmade rings of modeling clay (Staedtler). The weight treatments were distributed along a gradient (heavier rings at the bottom, and lighter at the top) positioned at 50%, 62.5% and 75% of the stem height. The weight of each ring also mimicked the biomass weight distribution or loading gradient in WT and *eki* trees. Diameter measurements were done under each ring position at the top (D7 at 75%, D6 at 62.5%, D5 at 50% of the stem height), and also in the last four internodes at the base: D4, D3, D2 and D1, D1 being the downmost one.

Condition 1 (C1): Trees were supported by three sticks next to the stem to prevent movement, and no weight manipulations were performed. Condition 2 (C2): Trees were prepared as in condition 1, but weight was applied as described above. Condition 3 (C3): Only one stick was added, 12 cm away from the stem; at the upper tip of the stick we added a metal wire ring (⌀=25 cm). Next, weight was applied as described above. This condition permits stem oscillations which are prevented in conditions 1 and 2. Condition 4 (C4): Pulling was performed using fishing lines (Sufix 832). Lines were attached to the stem with a thick protective parafilm layer. A metal structure was built on the top of trees (1.5 m) to allow us to hang Eppendorf tubes filled with weight (fishing sinkers). The amount and distribution of the weight was exactly the same as that calculated before for weight rings. WT (14-038-17) and *eki* (14-038-01) trees were intercalated within each treatment (Data S1).

Clonal propagation:

Dormant buds were collected as a starting material and clonal propagation was performed as previously described [25]. Briefly, explants were surface sterilized with 70% ethanol and cultured in 2.46/L Woody Plant Media (Duchefa), 0.5g/L MES monohydrate (Duchafa), 10g/L Sucrose

(Duchefa), 7g/L Agar (Difco), pH adjusted to 5.6 and autoclaved for 15 mins. Afterwards we added 1mg/L sterile filtered IAA for rooting and 0.8 mg/L BAP for shoot induction.

Time-lapse video:

WT and *eki* BC_1 trees were cut and regrown during three months by isolating a single standing stem. Since *eki* stems can collapse at any moment, WT and *eki* stems were grown with continuous support, and released only at the moment of shooting the time-lapse video (before the predicted collapse). Images were acquired with a Nikon D7100 camera in the time-lapse mode every 12 seconds, during 2.95 hs. Images are mirrored to present the WT on the left and *eki* on the right (30fps).

Anatomy analysis:

Samples used for cell number and cell size quantifications were fixed (1% glutaraldehyde, 4% formaldehyde, 0.05M sodium phosphate) and, after dehydration, were embedded in Leica HistoResin. 5 µm cross-sections were made using a Leica RM2165 rotary microtome with a Leica microtome blade. Slides were then stained in a 0.05% toluidine blue solution and imaged using a Leica 2500 microscope. Image analysis was done in Fiji[26] and cell segmentation and size quantification was done in LithoGraphX with Builder 1.2.2.7[27, 28] implementing the parameters available at the Github public repository (https://github.com/Zhangcambium2019/Zhang2019).

Transition Electron Microscopy (TEM) of tension wood samples was performed as previously described[29] without staining. Samples were processed and imaged at the Electron Microscopy Unit, Institute of Biotechnology, University of Helsinki. Wood samples for maceration of xylem fiber and vessel cells were oven dried (65 °C overnight). Then samples were treated with solution (1:1) of glacial acetic acid:H_2O_2 and heated at 95 °C until samples turned white. Before imaging samples were rinsed with water three times.

Pyrolysis-gas chromatography and mass spectrometry (Py-GC/MS):

50 µg (±10 µg) of ball-milled wood and bark powder was processed in a pyrolyzer equipped with an auto sampler (PY-2020iD and AS-1020E, Frontier Lab, Japan) connected to a GC/MS (7890A/5975C; Agilent Technologies, Santa Clara, CA, USA). The pyrolysate was separated using a DB-5MS capillary column (30 m. x 0.25 mm. i.d. 0.25µm film thickness). Next, samples were run through GC and MS using the program and settings previously described [30]. Analyses were done in the Biopolymer Analytical Platform (BAP) at Umeå Plant Science Centre/Swedish University of Agricultural Sciences (SLU), Sweden.

Monosaccharides and cellulose composition analysis of cell walls:

Alcohol insoluble residue (AIR) was prepared from fine wood and bark powder by extraction with 80% ethanol for 30 min at 95 °C, repeated with 70% ethanol, followed by chloroform:methanol (1:1)

and two washes with acetone at room temperature. In order to remove starch, the powder was treated overnight at 37 °C twice with α-amylase from pig pancreas (Roche 10102814001; 100 units per 100 mg of AIR) in a 0.1M potassium phosphate buffer, pH 7.0. Monosaccharide composition was analyzed using the trimethylsilyl (TMS) derivatization method. 500 µg of amylase-treated material and 30 µg of inositol, used as an internal standard, were methanolysed by treatment with 2M HCl/MeOH at 85 °C for 24hrs. Derivatization was carried out using Tri-sil reagent (3-3039 Sylon HTP kit, Supelco, Sigma-Aldrich) at 80 °C for 20 min as previously described[31] . The silylated monosaccharides were determined on a GC/MS (7890A/5975C; Agilent Technologies, Santa Clara, CA, USA) according to [32], using a J&W DB-5 MS column (Agilent Technologies) with the following oven program: 80 °C followed by a temperature increase of 20 °C/min to 140 °C for 2 min, then 2 °C /min to 200 °C for 5 min, then 30 °C/min to 250 °C for 5 min. The total run time was 47 min. Crystalline cellulose content was determined using the Updegraff method[33] followed by an anthrone assay to detect the released glucose[34]. Analyses were done in the Biopolymer Analytical Platform (BAP) at Umeå Plant Science Centre/Swedish University of Agricultural Sciences (SLU), Sweden.

Cell wall polymer immunolocalization:

Trees sections of WT and *eki* birch were dissected with razor blades (into sections several mm thick) and were immediately fixed in a solution consisting of 4% formaldehyde (freshly prepared from paraformaldehyde powder, Sigma) and 0,5% glutaraldehyde (Sigma) in a 0.1M phosphate buffer at pH 7. Fixation, dehydration and resin infiltration steps were all microwave (MW) assisted using a PELCO BioWave Pro (Ted Pella, Redding, CA). Fixation was realized at 150 W under vacuum (20Hg) (5x 1'). Samples were left in the fixative overnight at 4 °C and then washed 3 times in PBS. Samples were then processed through increasing dehydration steps (25%, 50%, 70%, 90%, 96%, 3x 100% Ethanol, vacuum 20Hg, MW 150 W 5'). Resin infiltration (LR White medium grade, Agar scientific) was then realized through increasing resin concentration: 33% resin in 100% ethanol, 66% resin in 100% ethanol, and 3 times 100% resin (20Hg, MW 200 W 5'). Samples were left overnight in 100% resin for effective penetration. Resin polymerization was subsequently realized at 60 °C over 17h. Semi-thin sections (1 µm) were then obtained with a Leica EM UC7 ultramicrotome. LM19 and LM20 Immunolocalization on the semi-thin sections was performed as follows: blocking step (BSA 2% in PBS, 1 mL per slide, 1 h RT); primary antibodies 1/10 in BSA 2% in PBS, 500 µL per slide, ON 4 °C (LM19/LM20[35], plantprobes, Leeds UK); 5 washes in BSA 2% in PBS (MW 150 W, 1'); secondary antibodies (Alexa Fluor 488 Goat anti-Rat IgM, ThermoFisher Scientific, A-21212) 1/100 in BSA 2% in PBS, 500 µL per slide, 2 h RT; 5 washes in BSA 2% in PBS (MW 150 W, 1'). Slides were finally mounted in a 1:1 solution of AF1 antifadent (Citifluor) with PBS containing calcofluor as a cell wall counterstaining and then imaged by confocal laser scanning microscopy (Zeiss LSM700). With the same procedure crystallin cellulose was detected using CBM3a [36]and

anti-6X His tag antibody and Alexa Fluor 488 Goat anti-Chiken IgY secondary antibody. The images contrast and brightness were equally adjusted in all immunolocalization figures including the negative controls.

Cryosections and staining:

Freshly sampled stems were kept in -80 °C until sectioning. A Leica CM3050S cryotome was set to -26 °C and 10 µm stem cross-sections were obtained and immediately mounted in a drop of water. Safranin (0.5% in 50% ethanol) and alcian blue (1% in water) were used for staining.

Atomic force microscopy (AFM):

AFM measurements across the wood forming zone was performed on stem cross sections from the internode 12 of WT and *eki* trees. The cross-sections were manually dissected, mounted on slides and kept in a humid chamber until analysis. The handmade cuts of approximately 300 µm were made using fresh Wilkinson Sword razor blades. All slides contained at least 3 WT and 3 *eki* cross-sections, and 3 independently grown clones of WT (14-038-17) or *eki* (14-038-01) trees were used. Additionally, sliced cross-sections were immobilized on glass slides and surrounded by stiff agarose. Measurement of cell wall properties alone was ensured by the suppression of turgor pressure by immersing all cuts in a hypertonic solution a minimum of 20 minutes before measurement (0.55M mannitol). AFM JPK Nanowizard was used for scanning. The scanning of wood-forming tissues was initiated at the inner border of the phloem fibers and moved 5 times towards the mature xylem. All sections were scanned from left to right, and stereomicroscope pictures of the initial and final cantilever position were acquired to later identify the corresponding tissues.

Data analysis was performed using the JPK Data Processing software (ver. Spm – 4.0.23, JPK Instruments AG, Germany), and Matlab was used to generate heatmaps of Young's modulus as well as to do the statistical analyses. The AFM data were collected following the same protocol as previously described[37]. The following cantilevers were used: "Nano World" (NanoWorld AG Headquarters, Neuchâtel, Switzerland) TL-NCH-20 tips with a spring constant of 10 – 130 N/m (those used were estimated to be 1.5 N/m) with Sphere Tips of a 25 µm radius. All force spectroscopy experiments were performed and calculated as previously described [37]; briefly, the rigidity of samples was determined as follows: an AFM cantilever loaded with a spherical tip was used to indent the sample over a 100 x 100 µm square area, then measurements were made within the area resulting in 10,000 force-indentation experiments; each force-indentation experiment was analyzed using a Hertzian indentation model to extrapolate the apparent Young's modulus, with each pixel in the rigidity map representing the Young's modulus from one force-indentation point.

The maximum force applied by the cantilever was set so as to perform a deformation approximately of 2 µm: Set point: 381.323 nN, Re.Setpoint: 4.500nN, z-length: 5, z-movement: constant speed, Extend Speed: 200, Sample Rate 8000. Results were discarded whenever sample movement or

outreach sample height was detected. Trees were grown in Helsinki and transported to Cambridge for analysis. The experiment was repeated once.

Tensile strength testing of full stems:

Three-point bending tests were performed to analyze the mechanical properties of the full stems using a Texture analyser TA.XT (Stable Micro Systems Ltd., Godalming, Surrey, U.K.). A 5 kg load cell was used. Previously, samples were prepared by selecting internodes of approximately the same diameter (2.83±0.27 mm) from a middle height along the stem of WT and *eki*. Samples were dried overnight at 65 °C. The measurement procedure was based on descriptions of similar tests by Horvath et al. (2010) and Sindhu et al. (2007), with modifications. As the TA.XTs three-point bending rig and probe (HDP/3PB) were too large to be used with these samples, a custom rig and probe with smaller dimensions were constructed. After attaching the fixture and the probe, a calibration was performed. The stem sample was placed on the fixture with a 25 mm gap width. The aluminum probe (width 1 mm) pushed down the sample in its middle. The speed of the probe was set to 1 mm/s. Three biological replicates and three technical replicates were measured. The sample diameter was 2.83±0.27mm. The Texture Exponent 32 software (version 6) recorded the force (g) and distance (mm) data. Hardness was determined as the force (g) required to break the sample. Brittleness was defined as the distance to break (mm), an indicator of how far a sample can be deformed before fracturing. Toughness was determined as the slope of these two (mm/g).

Ploidy estimation by flow cytometry:

Samples of ~1 cm^2 of leaf from in-vitro grown plant material were collected in a pre-chilled, clear, flat, glass petri-dish. The samples were chopped with razor blades in ≤60 seconds in woody plant buffer[38] with slight modifications (200mM Tris, 4 mM $MgCl_2$, 2 mM Na_2EDTA, 86 mM NaCl, 10 mM sodium metabisulfite, 1% PVP-40, 1% (v/v) Triton X-100 at pH 7.5 and stored at 4 °C) The samples were filtered through 40 µm nylon mesh filters (Corning™ C431750) and stained with 50 µg/ml propidium iodide (PI) and simultaneously with 50 µg/ml Rnase. Samples were incubated for 1 hour in darkness on ice. Flow cytometry was done using a BD LSR II flow cytometer (BD FACSDiva software 8.0.1) following the instrument's instructions. Rice leaves grown under long-day greenhouse conditions were used for the reference genome. The samples were kept on ice throughout the procedure.

DNA Sequencing:

Libraries for genome sequencing were prepared as described before [20] (page 26 section 1.3.1.2). The libraries had an insert size of approx. 350 bp and were paired-end (150 bp+150 bp) and were sequenced on a NextSeq 500 instrument (Illumina) at the DNA Sequencing and Genomics Laboratory, Institute of Biotechnology, University of Helsinki. Sequencing data has been deposited

in the NCBI sequence repository archive (SRA) under the BioProject ID: PRJNA545638. This data was used for Figure 2 and Figure S2.

Genome analysis, linkage mapping and QTL analysis:

Mapping reads to the genome

The backcross data was analyzed by mapping individual fastq files to the *B. pendula* genome[20] using bwa mem[39] and then producing sorted bam files using SAMtools[40].

Verifying tetraploidy

The SAMtools mpileup command and a custom script were used analyze the allele ratios of variant bi-allelic sites on the parental individuals. Only sites with total sequencing coverage between 12 and 100 and a minimum allele coverage of 3 were considered as variants. Density estimation and histogram production based on allele ratios was done using R[41].

Linkage mapping

Lep-MAP3 (LM3)[42] was used to construct a linkage map from the backcross data. The LM3 variant-calling pipeline was modified to call tetraploid genotypes. Specifically, the pileup2posterior.awk script was replaced with pileup2posterior_polyploid.awk and ParentCall2 with ParentCall2Ploidy. The pipeline only considers markers where parents have simplex markers, i.e. markers containing one different allele like AAAB for tetraploids with nucleotides A and B.

After the modified variant calling pipeline, the data was analyzed following the procedure for diploid data with LM3. Markers informative only in the mother or father were first clustered into linkage groups using SeparateChromosomes2 with an LOD score of 12 (lodLimit) and distortionLod=1 and more markers were added to these groups with JoinSingles2All with LOD 10. This yielded 28 linkage groups for paternal maps (two per chromosome of *B. pendula*) and 31 for maternal (two for chrs 2-14 and 5 for chr1). The 5 groups in chr1 were further grouped into two groups by extending the markers (by at most 5kb) in the two paternal linkage groups for chr1 and then running SeparateChromosomes2 on these markers without the distortionLod parameter (effectively a smaller LOD). The total number of paternal and maternal markers assigned to these groups were about 1.3M and 1.2M.

The markers in each of these linkage groups were ordered with OrderMarkers2 and Marey maps were plotted in R (Figure S2).

QTL analysis

LM3 outputs the segregation pattern for each marker. A custom script was used to calculate the LOD score between this pattern and the *eki*/WT pattern of each offspring. The closest pattern matching the phenotype in maternal maps had 12 (out of 60) differences, and there were 16 differences in paternal maps. The significance of these associations was calculated in R using a binomial distribution with a success parameter of 0.5 and with the number of unique markers (2740) as the Bonferroni (multiple test) correction term (R: 2740*2*pbinom(12, 60, 0.5)). The most significant region was located at the end of Chr11.

Genome anchoring

As each *B. pendula* chromosome corresponded to 4 linkage groups of 56, the *B. pendula* contigs were assigned to the 14 chromosomes based on the map (similarly as done before [20]) and placed and ordered based on marker positions. The Marey map (Figure S2) for the resulting genome was constructed using a custom R script.

Pooled data analysis

To verify the QTL results, the backcross offspring were analyzed as two pooled samples, one pool for all individuals showing WT phenotype and another for individuals with an *eki* phenotype. For both pools and each genomic position, the number of nucleotides, A, C, G and T, was calculated omitting positions where total counts were >1000. The likelihood ratio of the counts coming from one multinomial vs. two multinomial distributions (corresponding to one or two pools) was calculated. By randomly assigning phenotypes and calculating the LOD, a LOD limit of 13 was determined as best to find significant regions. The most significant region from this analysis overlapped with the QTL region in Chr11.

RNA-Seq analysis:

RNA extraction and sequencing

Samples from internode 2 (IN2) and from the bark (IN5bark) and xylem (IN5xylem) of internode 5 were collected from four WT and *eki* individuals growing in the greenhouse. All materials were immediately frozen in liquid nitrogen and stored at -80 °C for RNA extraction. RNA was extracted as described previously[43] and RNA quality was verified using an RNA Nano Chip from Agilent Technologies (US). The 78bp/74bp paired-end sequences were generated using the HiSeq2000 platform at the Sequencing and Genomics Laboratory, Institute of Biotechnology, University of Helsinki. Sequencing data has been deposited in the NCBI sequence repository archive (SRA) under the BioProject ID: PRJNA547511. This data was used for Figure 6 (Data S3).

Bioinformatics analysis

The raw sequencing data were first assessed using FastQC (v0.11.8, http://www.bioinformatics.babraham.ac.uk/projects/fastqc/). Residual ribosomal RNA (rRNA) contamination was filtered using SortMeRNA (v2.1)[44]. The removal of adaptors and low-quality reads and trimming of low-quality nucleotides were performed using Trimmomatic-0.35[45]. The quality of the processed reads was then assessed again with FastQC. High quality reads from each sample were mapped to the genome of *B. pendula* (v1.2) with corresponding gene model annotation using HISAT2 2.1.0[46]. Read counts per gene were generated using the featureCounts function in the Rsubread package. The transcripts per million (TPM) method was used to normalize the read count in each sample, and the trimmed mean of M-values (TMM) normalization method was used to equate the overall expression levels of genes between different samples. Differential expression analysis between mutant and wildtype for each type of sample was done using the DEseq2 R package[47]. DEGs were filtered based on having an absolute value of the $\log_2$fold change > 1 and an adjusted *p*-value < 0.05 (Data S3). Gene Ontology (GO) annotations for all genes were obtained as recently described[48], and GO functional enrichment analysis was performed by utilizing clusterProfiler R package[49].

Plots:

Box plots were generated using the online app "PlotsOfData"[50] and Venn Diagrams using the web-based tool "InteractiVenn" [51].

QUANTIFICATION AND STATISTICAL ANALYSIS

Statistical analysis was performed in Excel using two-tailed Student's t-test. The experimental and statistical details for each case can be found in the figures, figure legends, and supplementary data. The *p* values are provided in the figures, and supplementary data, statistically significant differences being $p \leq 0.05$.

DATA AND CODE AVAILABILITY

The DNA Sequencing data has been deposited in the NCBI sequence repository archive (SRA) under the BioProject ID: PRJNA545638. RNA Sequencing data has been deposited in the NCBI-SRA under the BioProject ID: PRJNA547511. This study did not generate code.

Supplemental Information

Video S1: Time-lapse video of WT and the collapsing phenotype of *eki*. Related to Figure 2.
To recapitulate the collapsing phenotype, single tree stems were regrown for three months with a supportive stacking. Stacking was removed before shooting the time-lapse. Before collapse *eki* trees strongly oscillated compared to WT, as result of the room ventilation combined with the

mechanical instability of the stem. The collapsing phenotype of *eki* occured within 3 hours (after support removal) resulting in a sharp bending at the stem base.

Data S1: Mechanical experiment and cell size contribution. Related to Figure 1 and 3. A, Raw measurement values of mechanical experiments. B, Quantitative and statistical summary of mechanical experiment. C, Radial contribution of xylem cells cross-sectional diameter in *eki.*

Data S2: Segregation of the mutant population and *EKI* locus analysis. Related to Figure 2. A, Deposited DNA Sequencing ID and final phenotype of BC_1 individuals. B, Phenotypic observations after seed germination in the individuals of the BC1 population. C, Candidate genes in the *EKI* locus (Chr11) and RNASeq based expression profiles. Genes present in the mapping window reportedly missregulated in *Arabidopsis* by touch.

Data S3: Gene expression analysis WT vs. *eki*. Related to Figure 6. A, Overview of sequencing read statistics in each sample and expression profile of all annotated *B.pendula* genes in BC1 WT and *eki* individuals. B, Subset of significant DEGs in WT vs. eki from the internode 2. C, Subset of significant DEGs in WT vs. eki from the internode 5 xylem tissues. D, Subset of significant DEGs in WT vs. eki from the internode 5 bark tissues.

References

1. Siedlecka, A., Wiklund, S., Péronne, M.-A., Micheli, F., Lesniewska, J., Sethson, I., Edlund, U., Richard, L., Sundberg, B., and Mellerowicz, E. J. (2008). Pectin methyl esterase inhibits intrusive and symplastic cell growth in developing wood cells of Populus. Plant Physiol. *146*, 554–565.
2. Serrano-Mislata, A., and Sablowski, R. (2018). The pillars of land plants: new insights into stem development. Curr. Opin. Plant Biol. *45*, 11–17.
3. Hamant, O., Heisler, M. G., Jönsson, H., Krupinski, P., Uyttewaal, M., Bokov, P., Corson, F., Sahlin, P., Boudaoud, A., Meyerowitz, E. M., et al. (2008). Developmental patterning by mechanical signals in Arabidopsis. Science *322*, 1650–1655.
4. Louveaux, M., Julien, J.-D., Mirabet, V., Boudaoud, A., and Hamant, O. (2016). Cell division plane orientation based on tensile stress in Arabidopsis thaliana. Proc. Natl. Acad. Sci. USA *113*, E4294-303.
5. Peaucelle, A., Braybrook, S. A., Le Guillou, L., Bron, E., Kuhlemeier, C., and Höfte, H. (2011). Pectin-induced changes in cell wall mechanics underlie organ initiation in Arabidopsis. Curr. Biol. *21*, 1720–1726.
6. Ko, J.-H., Han, K.-H., Park, S., and Yang, J. (2004). Plant body weight-induced secondary growth in Arabidopsis and its transcription phenotype revealed by whole-transcriptome profiling. Plant Physiol. *135*, 1069–1083.
7. Brown, C. L., and Sax, K. (1962). The influence of pressure on the differentiation of secondary tissues. Am. J. Bot. *49*, 683–691.
8. Gril, J., Jullien, D., Bardet, S., and Yamamoto, H. (2017). Tree growth stress and related problems. J. Wood Sci., 1–22.
9. Hongo, S., Sato, K., Yokoyama, R., and Nishitani, K. (2012). Demethylesterification of the primary wall by PECTIN METHYLESTERASE35 provides mechanical support to the Arabidopsis stem. Plant Cell *24*, 2624–2634.
10. Stovall, A. E. L., Anderson-Teixeira, K. J., and Shugart, H. H. (2018). Assessing terrestrial laser scanning for developing non-destructive biomass allometry. For. Ecol. Manag. *427*, 217–229.
11. Moulia, B., Bastien, R., Chauvet-Thiry, H., and Leblanc-Fournier, N. (2019). Posture control in

land plants: growth, position sensing, proprioception, balance, and elasticity. J. Exp. Bot.
12. Niklas, K. J., and Spatz, H.-C. (2004). Growth and hydraulic (not mechanical) constraints govern the scaling of tree height and mass. Proc. Natl. Acad. Sci. USA *101*, 15661–15663.
13. McMahon, T. (1973). Size and shape in biology. Science *179*, 1201–1204.
14. Coutand, C., Dupraz, C., Jaouen, G., Ploquin, S., and Adam, B. (2008). Mechanical stimuli regulate the allocation of biomass in trees: demonstration with young Prunus avium trees. Ann. Bot. *101*, 1421–1432.
15. Rowe, N., and Speck, T. (2005). Plant growth forms: an ecological and evolutionary perspective. New Phytol. *166*, 61–72.
16. Gerttula, S., Zinkgraf, M., Muday, G. K., Lewis, D. R., Ibatullin, F. M., Brumer, H., Hart, F., Mansfield, S. D., Filkov, V., and Groover, A. (2015). Transcriptional and hormonal regulation of gravitropism of woody stems in populus. Plant Cell *27*, 2800–2813.
17. Bastien, R., Bohr, T., Moulia, B., and Douady, S. (2013). Unifying model of shoot gravitropism reveals proprioception as a central feature of posture control in plants. Proc. Natl. Acad. Sci. USA *110*, 755–760.
18. Hamant, O., and Moulia, B. (2016). How do plants read their own shapes? New Phytol. *212*, 333–337.
19. Longman, K. A., and Wareing, P. F. (1959). Early induction of flowering in birch seedlings. Nature *184*, 2037–2038.
20. Salojärvi, J., Smolander, O.-P., Nieminen, K., Rajaraman, S., Safronov, O., Safdari, P., Lamminmäki, A., Immanen, J., Lan, T., Tanskanen, J., et al. (2017). Genome sequencing and population genomic analyses provide insights into the adaptive landscape of silver birch. Nat. Genet. *49*, 904–912.
21. Chehab, E. W., Yao, C., Henderson, Z., Kim, S., and Braam, J. (2012). Arabidopsis touch-induced morphogenesis is jasmonate mediated and protects against pests. Curr. Biol. *22*, 701–706.
22. Xu, Y., Berkowitz, O., Narsai, R., De Clercq, I., Hooi, M., Bulone, V., Van Breusegem, F., Whelan, J., and Wang, Y. (2019). Mitochondrial function modulates touch signalling in Arabidopsis thaliana. Plant J. *97*, 623–645.
23. Fernie, A. R. (2019). Making sense of the complex role of the mitochondria in mediating the plant touch response. Plant J. *97*, 621–622.
24. Jensen, G. S., Fal, K., Hamant, O., and Haswell, E. S. (2017). The RNA Polymerase-Associated Factor 1 Complex Is Required for Plant Touch Responses. J. Exp. Bot. *68*, 499–511.
25. Lemmetyinen, J., Keinonen-Mettälä, K., Lännenpää, M., von Weissenberg, K., and Sopanen, T. (1998). Activity of the CaMV 35S promoter in various parts of transgenic early flowering birch clones. Plant Cell Rep. *18*, 243–248.
26. Schindelin, J., Arganda-Carreras, I., Frise, E., Kaynig, V., Longair, M., Pietzsch, T., Preibisch, S., Rueden, C., Saalfeld, S., Schmid, B., et al. (2012). Fiji: an open-source platform for biological-image analysis. Nat. Methods *9*, 676–682.
27. Wunderling, A., Ben Targem, M., Barbier de Reuille, P., and Ragni, L. (2017). Novel tools for quantifying secondary growth. J. Exp. Bot. *68*, 89–95.
28. Home Page Available at: http://www.lithographx.com/ [Accessed April 24, 2019].
29. Lehringer, C., Daniel, G., and Schmitt, U. (2009). TEM/FE-SEM studies on tension wood fibres of Acer spp., Fagus sylvatica L. and Quercus robur L. Wood Sci. Technol. *43*, 691–702.
30. Gerber, L., Eliasson, M., Trygg, J., Moritz, T., and Sundberg, B. (2012). Multivariate curve resolution provides a high-throughput data processing pipeline for pyrolysis-gas chromatography/mass spectrometry. J. Anal. Appl. Pyrolysis *95*, 95–100.
31. Sweeley, C. C. (1963). Gas-Liquid Chromatography of Trimethylsilyl Derivatives of Sugars and Related Substances. Available at: https://pubs.acs.org/doi/abs/10.1021/ja00899a032

[Accessed March 25, 2019].
32. Sweeley, C. C., Elliott, W. H., Fries, I., and Ryhage, R. (1966). Mass spectrometric determination of unresolved components in gas chromatographic effluents. Anal. Chem. *38*, 1549–1553.
33. Updegraff, D. M. (1969). Semimicro determination of cellulose inbiological materials. Anal. Biochem. *32*, 420–424.
34. Scott, T. A., and Melvin, E. H. (1953). Determination of Dextran with Anthrone. Anal. Chem. *25*, 1656–1661.
35. Verhertbruggen, Y., Marcus, S. E., Haeger, A., Ordaz-Ortiz, J. J., and Knox, J. P. (2009). An extended set of monoclonal antibodies to pectic homogalacturonan. Carbohydr. Res. *344*, 1858–1862.
36. Blake, A. W., McCartney, L., Flint, J. E., Bolam, D. N., Boraston, A. B., Gilbert, H. J., and Knox, J. P. (2006). Understanding the biological rationale for the diversity of cellulose-directed carbohydrate-binding modules in prokaryotic enzymes. J. Biol. Chem. *281*, 29321–29329.
37. Peaucelle, A. (2014). AFM-based mapping of the elastic properties of cell walls: at tissue, cellular, and subcellular resolutions. J. Vis. Exp.
38. Pellicer, J., and Leitch, I. J. (2014). The application of flow cytometry for estimating genome size and ploidy level in plants. Methods Mol. Biol. *1115*, 279–307.
39. Li, H. (2013). Aligning sequence reads, clone sequences and assembly contigs with BWA-MEM. arXiv.
40. Li, H., Handsaker, B., Wysoker, A., Fennell, T., Ruan, J., Homer, N., Marth, G., Abecasis, G., Durbin, R., and 1000 Genome Project Data Processing Subgroup (2009). The Sequence Alignment/Map format and SAMtools. Bioinformatics *25*, 2078–2079.
41. R Core Team (2008). R: A language and environment for statistical computing. R Foundation for Statistical Computing, Vienna, Austria. . Available at: URL http://www.R-project.org/. [Accessed April 3, 2019].
42. Rastas, P. (2017). Lep-MAP3: robust linkage mapping even for low-coverage whole genome sequencing data. Bioinformatics *33*, 3726–3732.
43. Lim, K.-J., Paasela, T., Harju, A., Venäläinen, M., Paulin, L., Auvinen, P., Kärkkäinen, K., and Teeri, T. H. (2016). Developmental Changes in Scots Pine Transcriptome during Heartwood Formation. Plant Physiol. *172*, 1403–1417.
44. Kopylova, E., Noé, L., and Touzet, H. (2012). SortMeRNA: fast and accurate filtering of ribosomal RNAs in metatranscriptomic data. Bioinformatics *28*, 3211–3217.
45. Bolger, A. M., Lohse, M., and Usadel, B. (2014). Trimmomatic: a flexible trimmer for Illumina sequence data. Bioinformatics *30*, 2114–2120.
46. Kim, D., Langmead, B., and Salzberg, S. L. (2015). HISAT: a fast spliced aligner with low memory requirements. Nat. Methods *12*, 357–360.
47. Love, M. I., Huber, W., and Anders, S. (2014). Moderated estimation of fold change and dispersion for RNA-seq data with DESeq2. Genome Biol. *15*, 550.
48. Alonso-Serra, J., Safronov, O., Lim, K.-J., Fraser-Miller, S. J., Blokhina, O. B., Campilho, A., Chong, S.-L., Fagerstedt, K., Haavikko, R., Helariutta, Y., et al. (2019). Tissue-specific study across the stem reveals the chemistry and transcriptome dynamics of birch bark. New Phytol. *222*, 1816–1831.
49. Yu, G., Wang, L.-G., Han, Y., and He, Q.-Y. (2012). clusterProfiler: an R package for comparing biological themes among gene clusters. OMICS *16*, 284–287.
50. Postma, M., and Goedhart, J. (2019). PlotsOfData-A web app for visualizing data together with their summaries. PLoS Biol. *17*, e3000202.
51. Heberle, H., Meirelles, G. V., da Silva, F. R., Telles, G. P., and Minghim, R. (2015). InteractiVenn: a web-based tool for the analysis of sets through Venn diagrams. BMC Bioinformatics *16*, 169.

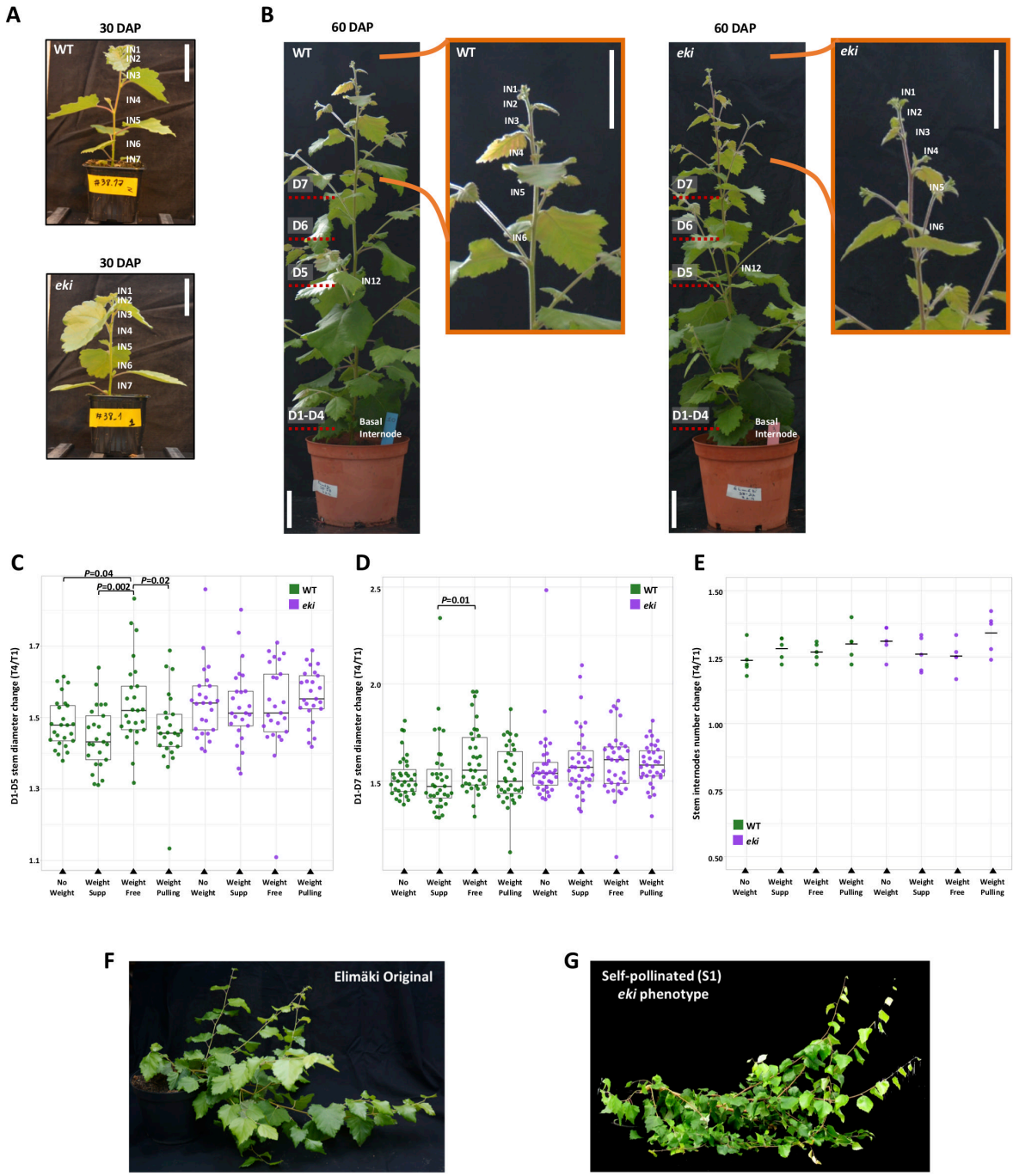

Figure S1. Developmental stages of trees and analysis vertical mechanical manipulations in WT and *eki*. Related to Figure 2 and 3. A) Localization of stem internodes used in the analysis of vascular phenotypes of 30 days after potting (DAP) (scalebar = 5cm.) **B)** Localization of stem internodes in trees 60 DAP, and stem positions measured during the mechanical treatments (D1-D7) (scalebar = 5cm.). **C)** Stem diameter change (equivalent to percentual growth rates: 1.5 = 50%) between the final and initial timepoints (T4/T1) using combined data from internodes D1-D5. **D)** Stem diameter change (equivalent to percentual growth rates: 1.5 = 50%) between the final and initial timepoints (T4/T1) using combined data from internodes D1-D7. In all boxplots, the box indicates the IQR, the whiskers show the range of values within 1.5*IQR, and a horizontal line indicates the median. **E)** The change in the number of internodes between then final and initial timepoints (T4/T1), with a horizontal line indicating the median. Each experimental setup consisted of 5 biological replicates per treatment. *p* values of statistically significant differences ($p \leq 0.05$) among treatments within

each genotype are indicated. **F)** Phenotype of three months old clonally propagated *Elimäki Original* trees after collapse **G)** Phenotype of self-pollinated EO progenies (S1) after collapse.

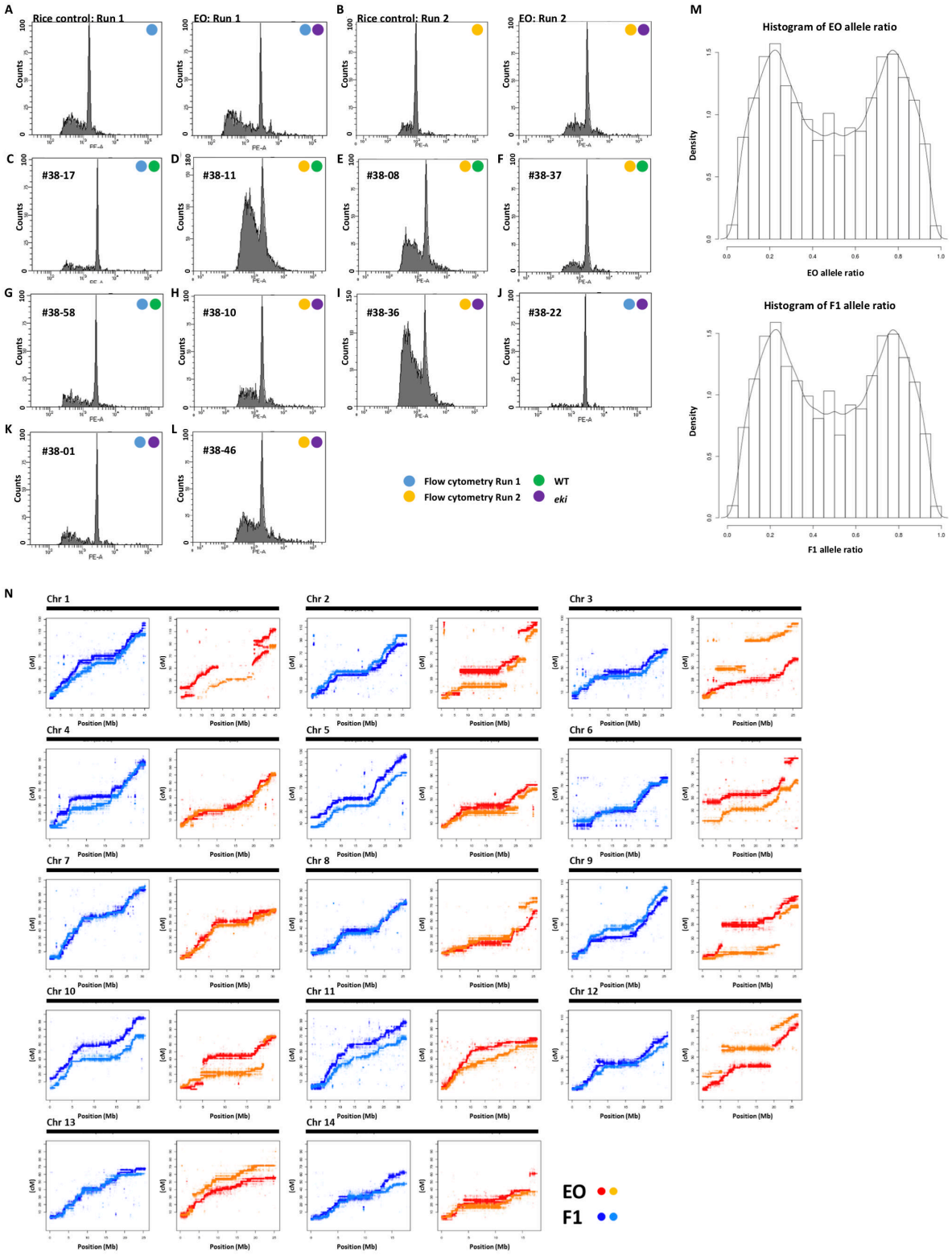

Figure S2: Ploidy analysis and *B. pubescens* Marey map. Related to Figure 2. A-L) Flow cytometry based ploidy analysis: The analysis was performed in two batches, each with the rice and Elimäki Original (EO) as controls **A)** Left: *Oryza sativa* was used as a diploid genome control (430Mb). Right: EO shows a peak at double the genome size of rice; similar results

have been reported before[20]. **B)** A second run of the same controls shown in (A). **C-L)** The remaining plots correspond to individuals from the BC_1 population showing peaks of genome sizes similar to their corresponding EO control. wild type trees: #38-17, #38-11, #38-09, #38-37, #38-58; **H-L)** *eki* trees: #38-10, #38-36, #38-22, #38-01, #38-46. **M)** Allele ratios at bi-allelic variants for EO and F1 individuals. Peaks at about 1/4 and 3/4 correspond to bi-allelic tetraploid markers of types AAAB and ABBB, thus supporting the tetraploidy of these individuals. **N**) Marey maps for all 56 linkage groups distributed across 14 chromosomal groups (Chr). Note that each *B. pendula* chromosome has 4 linkage groups, two maternal from EO (red and orange) and two paternal from F1 (light and dark blue).

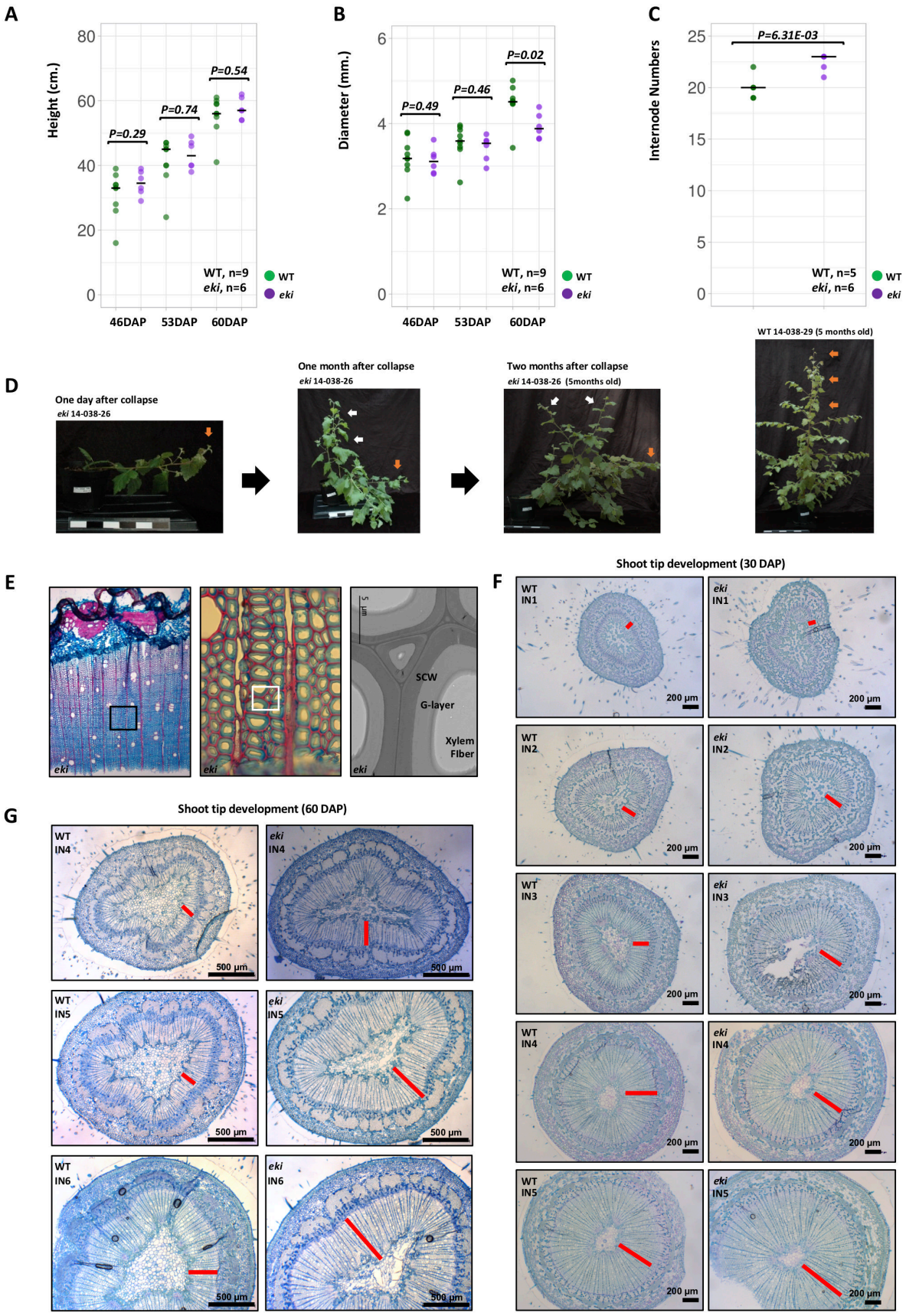

Figure S3: Developmental phenotypes before and after stem collapse. Related to Figure 2 and 3. A-C) Plots of the growth dynamics of WT vs. *eki* before collapse, at 46, 53 and 60 days after potting (DAP), showing the total height **(A)** and the diameter 10 cm above the base

(B). WT, n = 9; *eki*, n = 6 trees. **C)** Total internode numbers of trees before collapse. In all dot plots, the horizontal line indicates the median. Statistically significant differences between WT and *eki* ($p \leq 0.05$) were determined by a two-tailed Student's t-test and are indicated in the plots. n=biological replicates, n_n=samples D) One day after collapse, *eki* trees show a gravitropic response as the main shoot tip bends upwards (orange arrow); the following month, initiation of side-branches was triggered near the base of the stem (white arrows). While these branches initially displayed a vertical orientation, their ability to stand upright was eventually compromised resulting in a successive collapse, and finally leading to a highly branched, bush-like architecture **E)** Two months after collapse, the anatomy of the main stem in *eki* displayed a large accumulation of tension wood, as revealed in cryosections stained with alcian blue and safranin. TEM images show the normal development of G-layers on the inner side of secondary cell walls (SCW). **F)** Cross-sections stained with toluidine blue show the developmental progression of internodes at the shoot apex in 30 DAP trees, with the *eki* cross-sections revealing larger xylem expansion (quantified in Figure 3). **G)** Cross-sections stained with toluidine blue show the developmental progression of internodes at the shoot apex in 60 DAP trees, with *eki* cross-sections revealing earlier xylem expansion.

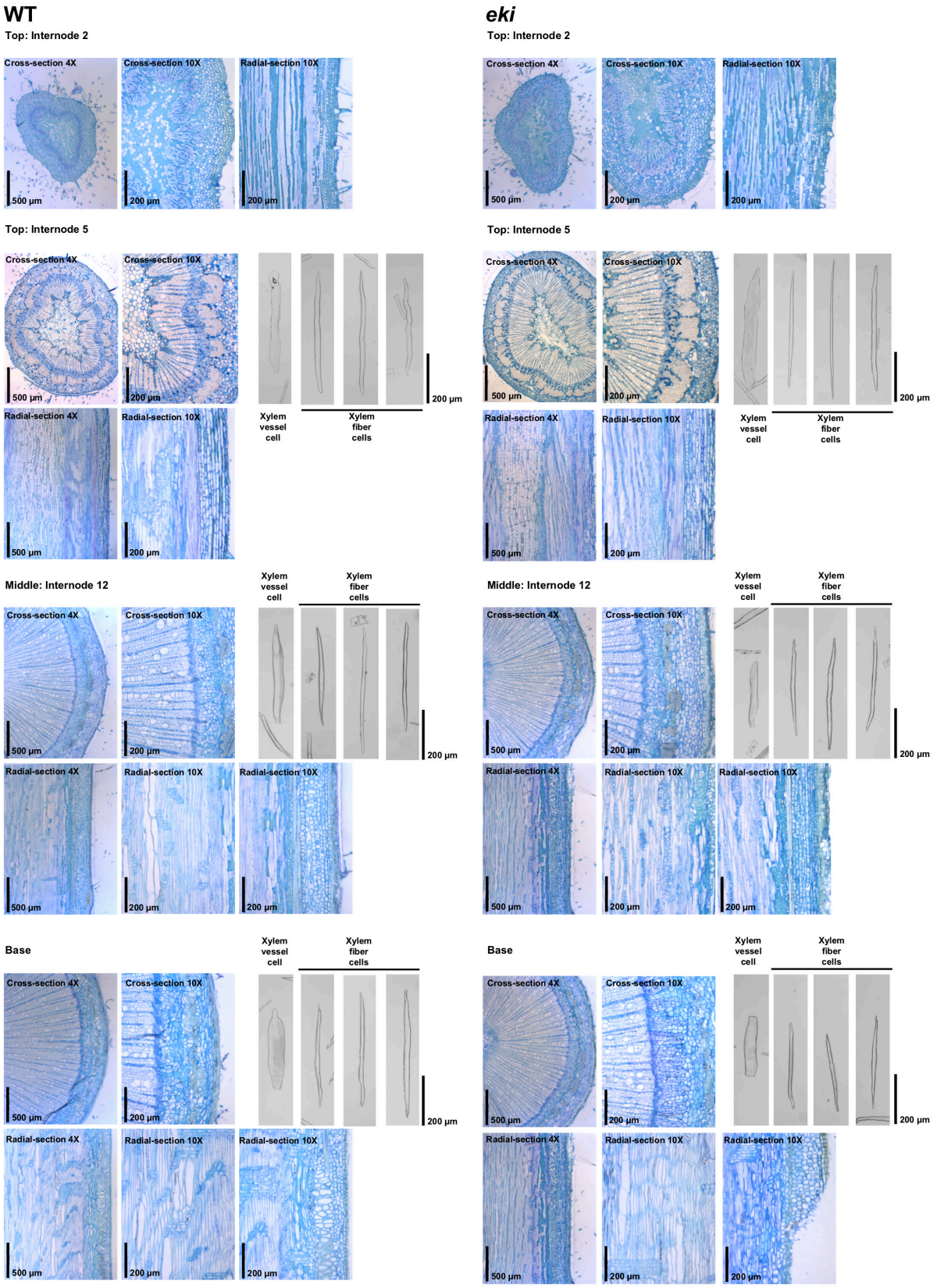

Figure S4: Anatomical views of wood formation in WT and *eki*. Related to Figure 3. Dissected main stems are shown in cross-sections and radial sections stained with Toluidine blue. The internode 2 shows a cambial organization in bundles (procambium), instead secondary growth was observed at the internode 5 where a fully connected cambial ring produces secondary xylem and phloem tissues. Single xylem vessel and fiber cells were obtained by maceration.

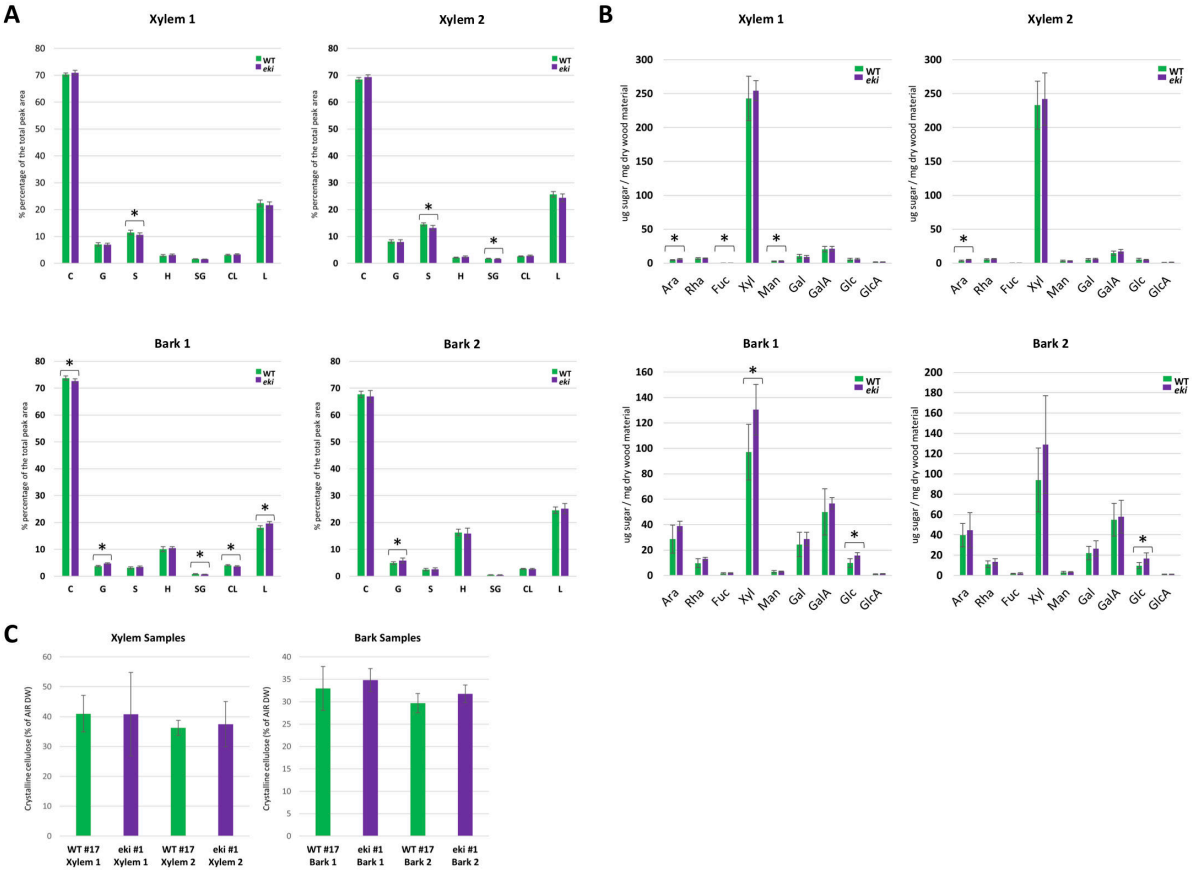

Figure S5: Cell wall profiling in young and mature tissues. Related to Figure 5. A) Pyrolysis-GC/MS analysis of xylem and bark from WT and *eki.* Comparison of identified peak areas, with values showing the percentage of the total peak area. Xylem 1 and Bark 1: Xylem and bark tissues from internodes 6-7-8. Xylem 2 and Bark 2: Xylem and bark tissues from internodes 9-10-11. C: combined peaks attributable to carbohydrates, G: peaks attributable to guaiacyl lignin, S: peaks attributable to syringyl lignin, H: peaks attributable to *p*-hydroxyphenyl lignin, SG: S/G ratio, CL: C/L ratio, L: combined peaks attributable to lignin. Bars represent the average value and error bars indicate the standard deviation of 3 biological replicates and 3 technical replicates. (*) Asterisks indicate statistically significant differences (p <0.05 in two-tailed Student's t-test) comparing WT vs. *eki*. **B)** Monosaccharide composition analysis of AIR by TMS derivatization with GC/MS. Xylem 1 and Bark 1: Xylem and bark tissues from internodes 6-7-8. Xylem 2 and Bark 2: Xylem and bark tissues from internodes 9-10-11. Ara: arabinose, Rha: rhamnose, Fuc: Fucose, Xyl: xylose, Man: mannose, Gal: galactose, GalA: galacturonic acid, Glc: glucose, GlcA: glucuronic acid. Bars represent the average value and error bars indicate the standard deviation of 3 biological replicates and 2 technical replicates. (*) Asterisks indicate statistically significant differences (p <0.05 in two-tailed Student's t-test) comparing WT vs. *eki*. **C)** Updegraff cellulose determination in WT and *eki*. Xylem 1 and Bark 1: Xylem and bark tissues from internodes 6-7-8. Xylem 2 and Bark 2: Xylem and bark tissues from internodes 9-10-11. Bars represent the average value and error bars indicate the standard deviation of 3 biological replicates and 3 technical replicates. No statistically significant differences (p <0.05) were found in a two-tailed Student's t-test comparing WT vs. *eki*.

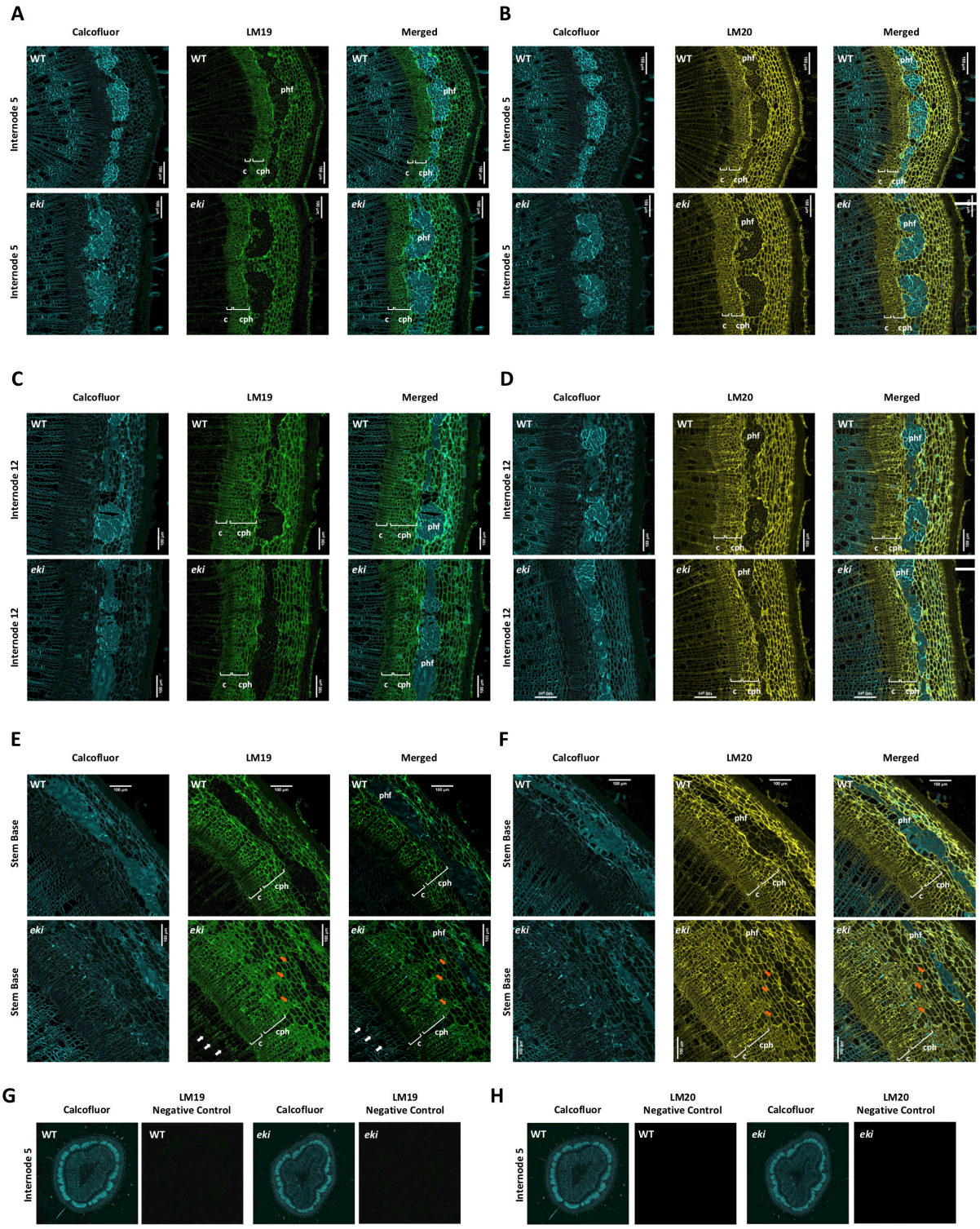

Figure S6: Developing xylem and phloem tissues retain PCW characteristics in *eki*. Related to Figure 5. Immunolocalization in stem cross from internode 5 **(A, B)**, internode 12 **(C, D)** and the oldest internode at the stem base **(E, F)**. Images show calcofluor white counterstaining (cyan), and LM 19 (green) or LM 20 (yellow) immunolocalization. Brackets in the figures correspond to: cambium (c), conductive phloem (cph). Phloem fibers (phf). White arrows indicate the LM19 labeling in xylem. In WT trees the conductive phloem connects cambium and phloem fibers, but extra parenchymatous cells labeled by LM19 and LM20 can be found in *eki* (orange arrows). Notice that this phenotype was more present in cross-sections from the base of the stem. **G-H)** Negative controls were performed without the primary

antibodies, and with the secondary antibody. Calcofluor white was used as counterstaining (cyan).